Pacific Northwest
NATIONAL LABORATORY

PNNL-30523

Future Response of Coastal Wetlands to Environmental Stresses: Algorithm Comparison of Numerical Models

October 2020

1Zeli Tan
2Chang Liao
3L. Ruby Leung
4Vanessa L. Bailey

U.S. DEPARTMENT OF ENERGY

Prepared for the U.S. Department of Energy
under Contract DE-AC05-76RL01830

DISCLAIMER

PACIFIC NORTHWEST NATIONAL LABORATORY
operated by
BATTELLE
for the
UNITED STATES DEPARTMENT OF ENERGY
under Contract DE-AC05-76RL01830

Printed in the United States of America

Available to DOE and DOE contractors from
the Office of Scientific and Technical
Information,
P.O. Box 62, Oak Ridge, TN 37831-0062
www.osti.gov
ph: (865) 576-8401
fox: (865) 576-5728
email: reports@osti.gov

Available to the public from the National Technical Information Service
5301 Shawnee Rd., Alexandria, VA 22312
ph: (800) 553-NTIS (6847)
or (703) 605-6000
email: info@ntis.gov
Online ordering: http://www.ntis.gov

PNNL-30523

Future Response of Coastal Wetlands to Environmental Stresses: Algorithm Comparison of Numerical Models

October 2020

1Zeli Tan
2Chang Liao
3L. Ruby Leung
4Vanessa L. Bailey

Prepared for
the U.S. Department of Energy
under Contract DE-AC05-76RL01830

Pacific Northwest National Laboratory
Richland, Washington 99354

Report

Abstract

Introduction and Objectives

This report describes research performed under the PNNL LDRD Project PN19061/3150: Future Response of Coastal Wetlands to Environmental Stresses: Algorithm Comparison of Numerical Models. The objective of this work is to build a model comparison platform for coastal wetland eco-geomorphological processes to evaluate the algorithm-level uncertainties in coastal wetland modeling. Further, this project is to identify the processes that need more research to better predict future response of coastal wetlands to environmental changes. This work will pave ways for integrating coastal wetlands into Earth system models.

Technical Approach

The basic technical approach is developing a multiple-algorithm model framework of coastal wetlands that represents coastal hydrodynamics (such as water level, significant wave height and bottom shear stress) and four eco-geomorphological processes: mineral accretion, organic matter accretion, storm surge erosion and landward migration.

Results

The capability of this model approach to reveal the structural uncertainties of coastal wetland models was demonstrated. The model was successfully applied at three representative coastal wetland sites (Venice Lagoon, Plum Island Estuary and Hunter Estuary) for simulating hydrodynamics, mineral accretion and organic matter accretion. Through model-data comparison, the model is shown to well capture the dynamics of hydrodynamical and eco-geomorphological conditions in the study sites. Importantly, analysis of the multiple-algorithm simulations suggests that differences in the process representation of mineral and organic matter accretion may contribute to the recent contradicting predictions of coastal wetland evolution under accelerated sea-level rise.

1. Introduction

Coastal wetlands such as tidal marshes and mangroves are valued for providing many important ecosystem services, including coastline protection, storm surge attenuation, wildlife habitat, water quality improvement, and also carbon sequestration (Aburto-Oropeza et al., 2008; Macreadie et al., 2019; Temmerman et al., 2013; Teuchies et al., 2013). Despite the resilience of these ecosystems to past fluctuations in sea level and climate (Cahoon et al., 2006), recent observations of local wetland loss raise concerns over their acclimation to intensified natural and human-induced disturbances, such as sea level rise (SLR), storm surge, sediment reduction, eutrophication and drought (Blum & Roberts, 2009; Crosby et al., 2016; Deegan et al., 2012; Kirwan & Megonigal, 2013). Eco-geomorphological processes such as mineral accretion, organic matter (OM) accretion, landward migration and storm surge erosion have crucial influence on the evolution of coastal wetlands (Craft et al., 2009; Howes et al., 2010; Kirwan et al., 2016; Leonardi et al., 2015; Schuerch et al., 2018). Therefore, many numerical models have been developed in recent decades to simulate the dynamics of coastal wetland eco-geomorphology under the current environmental conditions and their response to future changes (D'Alpaos et al., 2011; Fagherazzi et al., 2012; Kirwan et al., 2010; Marani et al., 2007; Mcleod et al., 2010; Rodríguez et al., 2017).

Although previous numerical efforts have greatly advanced our understanding of the response of coastal wetlands to changing environment (Kirwan & Mudd, 2012; Leonardi et al., 2015; Mariotti & Fagherazzi, 2010; Reyes et al., 2000), important knowledge gaps remain. For example, existing numerical models of coastal wetland eco-geomorphology differ importantly in complexity and structure (Fagherazzi et al., 2012; Mcleod et al., 2010) and they have largely provided contradicting predictions on coastal wetland evolution under accelerated SLR (Craft et al., 2009; Kirwan et al., 2010, 2016; Rodríguez et al., 2017; Schuerch et al., 2018). It is thus critical to understand the structural uncertainty of these numerical models for model improvement and applications, similar to efforts undertaken to address uncertainties in other Earth system processes (Guseva et al., 2020; Huntzinger et al., 2013; Jin et al., 2016; Schellnhuber et al., 2014; Tan et al., 2018). Such work also aligns with the interest of the scientific community to represent the function and sensitivity of coastal ecosystems in Earth system models (ESMs) (Ward et al., 2020).

A few studies have advanced understanding of the uncertainty of coastal wetland eco-geomorphology models through model comparison (Kirwan et al., 2010) or model review (Fagherazzi et al., 2012; Mcleod et al., 2010). However, model comparison and review can only provide limited understanding of how structural model uncertainty maps onto uncertainty in the relevant model projections (Fisher & Koven 2020). First, previous model reviews mostly focused on analyzing eco-geomorphology models in terms of their capability and complexity, inputs requirements, spatial- and temporal-scale accountability, and practical applicability instead of their fidelity in simulating coastal wetland dynamics in diverse environmental conditions (Fagherazzi et al., 2012; Mcleod et al., 2010). Second, previous model comparison experiments were never implemented at the process level so the uncertainties associated with individual processes could not be isolated (Kirwan et al., 2010). Third, previous model comparison experiments were only implemented at very few sites (Kirwan et al., 2010) and did not include our updated understanding of coastal wetland eco-geomorphology (Schuerch et al., 2018).

To fill the aforementioned gaps, we developed an algorithm-level model comparison framework to investigate the structural uncertainty in representing four coastal wetland eco-geomorphological processes in widely-used numerical models: mineral accretion, OM accretion, landward migration and storm surge erosion. This algorithm-level approach has been found promising for assessing a particular process in numerical models (Donatelli et al., 2014; Jin et al., 2016; Tan et al., 2018). Through this work, we aim to 1) test the applicability of the algorithm-level framework for modeling coastal wetlands in diverse environments and 2) link the structural uncertainty of the four eco-geomorphology processes with uncertainty in the model response to SLR. This modeling work will also pave the way for appropriate representation of coastal wetland eco-geomorphology in ESMs and enable ensemble predictions of coastal wetland evolution. Our analysis focused on modeling mineral and OM accretion. Although the algorithms of landward migration and storm surge erosion have been implemented in the framework, their analysis will be done in the future.

2. Methods and material

2.1. Model description

We developed a Multiple-Algorithm Coastal wetland Eco-geomorphology Simulator (MACES) model framework to assess the impact of structural uncertainty of eco-geomorphology models on the prediction of coastal wetland evolution under intensified natural and human-induced disturbances. The MACES model consists of two components (Figure 1): a one-dimensional (1-D) transect-based hydrodynamic module (MACES-hydro) and four eco-geomorphology modules with multiple algorithm implementations (MACES-geomor). MACES-hydro simulates water level, tide velocity, significant wave height, bottom shear stress, suspended sediment and other hydrodynamic conditions in a coastal transect along the elevation and land cover gradient with water level at the seaward boundary and wind speed over the transect as inputs (Figure 2). Based on the simulated hydrodynamics, MACES-geomor calculates sediment deposition and OM burial at each grid cell of the coastal transect and lateral erosion at the wetland edge grid cell. At the end of each year, MACES updates the transect elevation profile and land cover. A basic feature of MACES is that different combinations of algorithms within four eco-geomorphology modules can be configured to test different model structures and evaluate their performances.

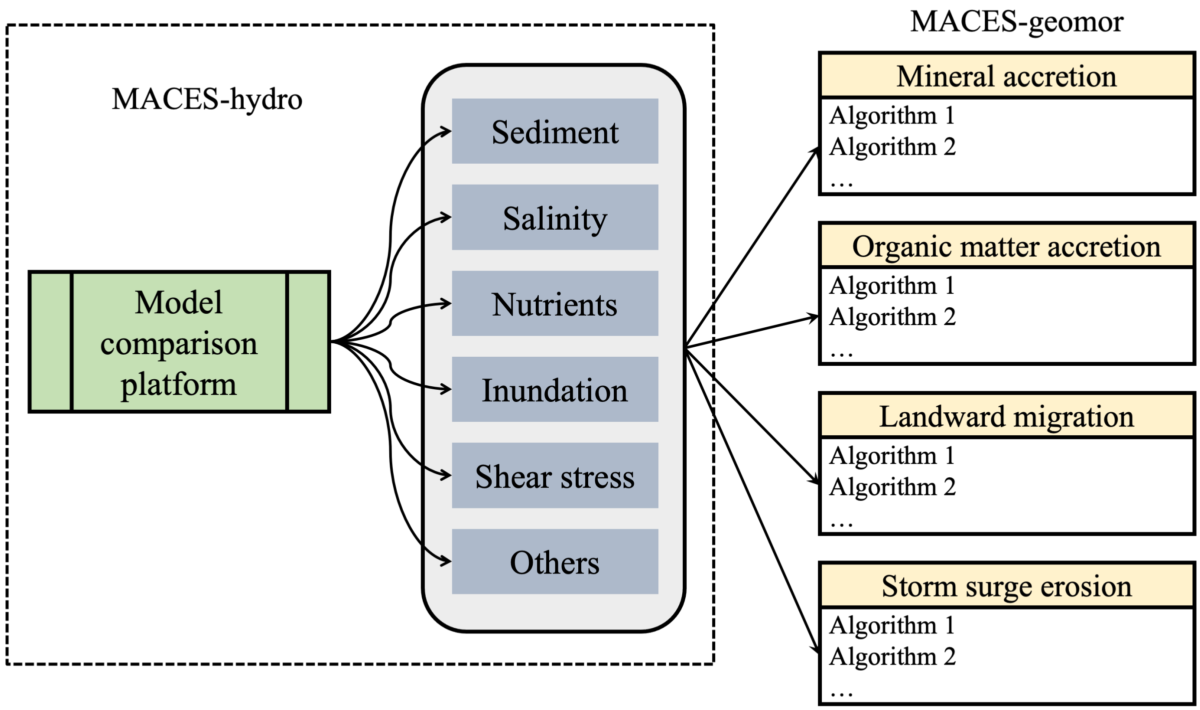

Figure 1. Model framework for algorithmic comparison of model response of coastal wetland to future environmental stresses. The model comparison platform builds on a 1-D coastal hydrodynamic model which simulates the dynamics of sediment, salinity, nutrients, water inundation, bottom shear stress and other hydrodynamic processes over three coastal landscapes.

The 1-D transect-based hydrodynamics in MACES-hydro consists of a tide propagation component, a wind-induced wave generation and propagation component and a particle transport component which are mainly based on the work of Tambroni & Seminara (2012) and Carniello et al. (2005) for modeling the cross-section averaged physical variables over coastal landscapes. We chose the 1-D hydrodynamic model over more advanced two-dimensional (2-D) or three-dimensional (3-D) hydrodynamic models for two reasons. First, the prominent features of coastal wetlands (such as tidal channels and microtopography) that 2-D and 3-D hydrodynamic models can represent are usually at spatial scales of meters, which are much finer than the spatial resolution of current and even future ESMs. Second, compared to 2-D and 3-D hydrodynamic models, 1-D hydrodynamic models can be much more easily deployed for global simulations. In MACES-hydro, tide propagation is governed by the classical continuity and the Saint Venant equations, which express the principles of mass and momentum conservation, and the primitive formulation of Mudd et al. (2004) is used to represent the impact of bed roughness and vegetation stem size and density on tidal current friction. Wave generation and propagation in shallow waters is governed by the conservation of the wave action based on the linear wave theory. Wave energy is generated by wind shear stress and dissipated by bottom friction, white capping and depth-induced breaking. Both tidal currents and wind wave contribute to the production of bottom shear stress with the nonlinear interaction between the two forces represented using the empirical formulation of Soulsby (1997). The concentration of suspended sediment in the tidal water is governed by the advection-dispersion continuity equation (Maan et al., 2015) with vertically averaged sediment erosion and deposition determined by MACES-geomor.

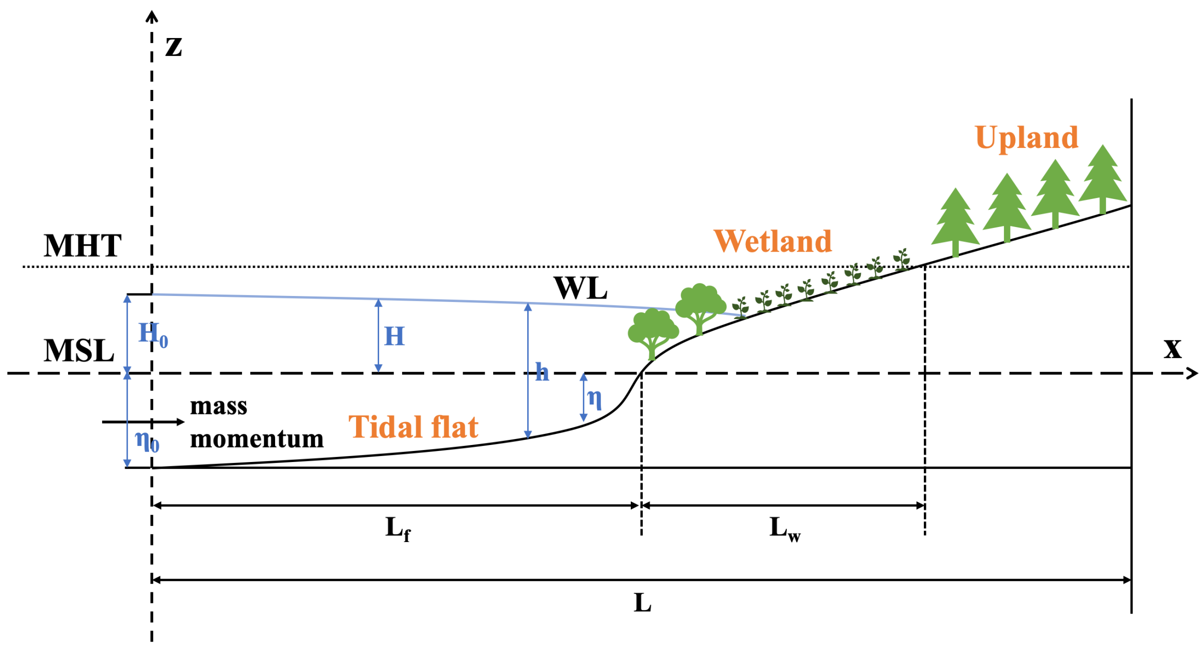

Figure 2. Sketch of the coastal system and notations. L denotes the 1-D transect domain of coastal landscapes with L_f as the domain of tidal flats and L_w as the domain of coastal wetland. MSL is mean sea level, MHT is mean high tide water level, and WL is water level. The notations of H, h and η represent water level relative to MSL, water depth and bottom elevation relative to MSL. H_0 is the water level at the seaward boundary and η_0 is the bottom elevation at the seaward boundary.

MACES-geomor includes seven numerical algorithms for mineral accretion, four numerical algorithms for OM accretion, one numerical algorithm for storm surge erosion (Leonardi et al., 2016) and three numerical algorithms for landward migration (Reyes et al., 2000; Rodríguez et al., 2017; Schuerch et al., 2018), respectively. In addition, for OM accretion, storm surge erosion and landward migration, another numerical algorithm corresponding to the null hypothesis of each process is included. The null hypothesis was added to test whether the examined eco-geomorphological process is insignificant for the evolution of coastal wetlands. Algorithms were selected through literature review based on three criteria. First, they have previously been successfully applied in multiple studies (ideally in wetlands located in different environmental conditions). Second, the algorithms have substantial differences in mathematical formulation and conceptual understanding. Third, they are compatible to the 1-D hydrodynamic model. Table 1 summarizes all the MACES-geomor algorithms and their characteristics.

Table 1. Summary of MACES eco-geomorphology algorithms.

Eco-geomorphology	Category	Algorithm
Mineral accretion	Only sediment deposition	F06 (French, 2006); T03 (Temmerman et al., 2003)
	Both sediment deposition and vegetation trapping	KM12 (Kirwan & Mudd, 2012)
	Both sediment deposition and erosion	F07 (Fagherazzi et al., 2007); VDK05 (van de Koppel et al., 2005)
	Sediment deposition, vegetation trapping and erosion	DA07 (D'Alpaos et al., 2007); M12 (Morris et al., 2012)
OM accretion	No growth seasonality and static shoot:root ratio	M12 (Morris et al., 2012)
	Growth seasonality and static shoot:root ratio	DA07 (D'Alpaos et al., 2007); K16 (Kakeh et al., 2016)
	Growth seasonality, dynamic shoot:root ratio and dynamic carbon turnover	KM12 (Kirwan & Mudd, 2012)
Storm surge erosion	Linear function of wave power	L16 (Leonardi et al., 2016)
Landward migration	Inundation and salinity thresholds	R20 (Reyes et al., 2000); R17 (Rodríguez et al., 2017); S18 (Schuerch et al., 2018)

2.2. Numerical methods

We employed a 1-D Godunov-type central-upwind scheme (Kurganov & Levy, 2002) to discretize the spatial domain of the Saint Venant equations which include source terms due to bottom topography, the wave equation and the particle transport equation. This finite volume scheme introduces a linear piecewise approximation to each grid cell with the Superbee slope limiter (Roe, 1986) to achieve the solutions of both second-order accuracy in space and diminishing total variation. Because this scheme is very effective in suppressing spurious oscillation of the simulated water level at the periodically flooded areas, it has been widely used as the numerical solver for coastal hydrodynamics (Liang & Marche, 2009). After spatial discretization, we employed a fourth-order adaptive Runge-Kutta-Fehlberg method to discretize the hydrodynamic equations in the time domain to achieve second-order accuracy in time (Burden et al., 1978). In addition, to avoid negative particle concentrations, we incorporated a scheme described by Tan et al. (2015) into the Runge-Kutta-Fehlberg method to recursively curtail the running time step when large negative concentrations occur, until the negative values are small enough to be assigned safely as zero.

One prominent feature of MACES is the use of a hybrid Fortran and Python programming approach to balance computational efficiency with software usability. The computational-intensive hydrodynamic module was written in Fortran and then converted to a Python package using f2py (Python Software Foundation, Fredericksburg, VA, USA). All the other modules, including eco-geomorphology, I/O and settings, were written in Python 3 directly. As such, new algorithms of eco-geomorphology can be easily integrated into MACES in the future. Model input and output files are written in the NetCDF and Excel format and model settings are written in the user-friendly XML (Extensible Markup Language) format.

2.3. Model calibration and evaluation

Model calibration of different MACES-geomor algorithms was conducted using the Python-version Parameter ESTimation tool (PyPEST). The PyPEST tool was developed by Liao et al. (2019) based on the model-independent parameter estimation code PEST (Doherty et al., 1994). PyPEST carries out the calibration process iteratively with six steps (parameter generation, model configuration, input data generation, model run in parallel, output extraction, and output post-processing) until the user-defined cost function threshold criteria is met (Figure 3). Depending upon data availability at different sites, different combinations of observed dataset were used to calibrate different geomorphology module algorithms with consideration of module dependency. For example, observed long-term mineral accretion rate and suspended sediment concentrations were used to calibrate the mineral accretion algorithms. And observed long-term OM accretion rate and aboveground biomass were used to calibrate the OM accretion algorithms.

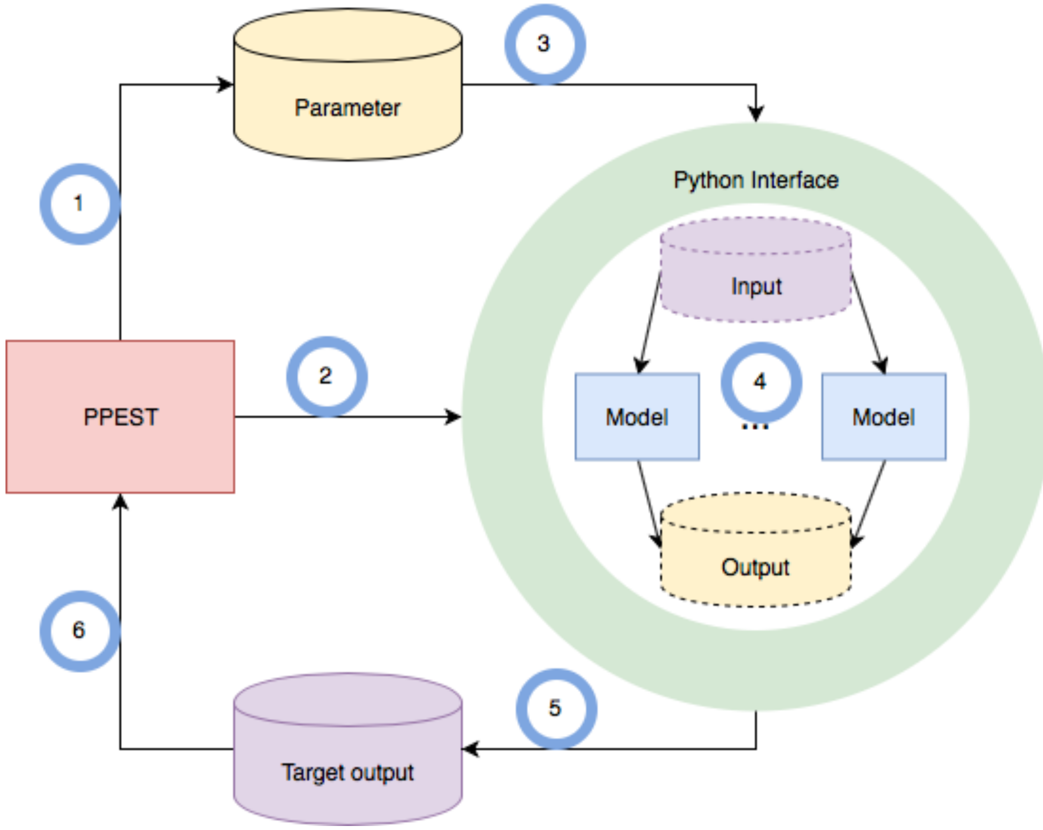

Figure 3. Illustration of the PyPEST workflow. PyPEST follows several steps indicated by the indices within circles. (1) PPEST (parallel version of PEST) generates new parameters; (2) PyPEST calls model interface of MACES; (3) model interface converts parameters into model inputs; (4) PyPEST runs MACES in parallel; (5) model interface extracts model outputs; (6) PPEST collect outputs for next iteration.

MACES-hydro was validated against observed or benchmark water level, significant wave height, suspended sediment and/or bottom shear stress without calibration. Because the related observations and benchmark estimates usually cover only a few days, during the MACES-hydro validation the model was only run for a few weeks. For MACES-geomor, we expect that most of the algorithms can reproduce the observed eco-geomorphology by calibration, so we did not focus our analysis on validating the individual algorithms explicitly. Instead, we focused on analyzing how the simulation uncertainty of fine spatiotemporal eco-geomorphology dynamics maps to the prediction uncertainty of long-term coastal wetland evolution. For example, although two algorithms might both reproduce the observed mineral accretion which is the long-term average of net sediment deposition over a saltmarsh site after calibration, they could differ importantly in simulating the elevation and distance gradient of sediment deposition along the transect of varied land cover and thus predict conflicting saltmarsh evolution under SLR (Tambroni & Seminara, 2012).

2.4. Model input and evaluation data

We evaluated the model at three representative coastal wetland sites with two located in midlatitude and one located in subtropics: Venice Lagoon, Plum Island Estuary and Hunter Estuary (Table 2). Venice Lagoon is a microtidal wetland with a large central waterbody and extensive intertidal salt marshes. The dominant saltmarsh species include *Limonium serotinum*, *Puccinellia palustris*, *Arthrocnemum fruticosum* and *Spartina maritima*. The long-term mineral and OM accretion rate of the saltmarsh are 3.5 mm yr^{-1} and 132 gC m^{-2} yr^{-1}, respectively (Bellucci et al., 2007; Roner et al., 2016). Plum Island Estuary is a macrotidal wetland with extensive areas of productive, tidal marshes. The dominant saltmarsh species include *Spartina alterniflora* at lower elevations and *Spartina patens* at higher elevations. The long-term mineral accretion rate can be as high as 6.9±0.9 mm yr^{-1} (Wilson et al., 2014) and the long-term OM accretion rate is 69.9±9.4 gC m^{-2} yr^{-1} (Wang et al., 2019). Hunter Estuary is a microtidal wetland with grey mangrove *Avicennia marina* at lower elevations and *Sporobolus virginicus*–*Sarcocornia quinqueflora* mixed saltmarsh at higher elevations. The mineral accretion of mangroves and saltmarsh are 3.66 mm yr^{-1} and 3.37 mm yr^{-1}, respectively (Howe et al., 2009). The OM accretion of mangroves and saltmarsh are 105 gC m^{-2} yr^{-1} and 137 gC m^{-2} yr^{-1}, respectively (Howe et al., 2009).

To simulate the hydrodynamics and eco-geomorphology of coastal wetlands, MACES is driven by the seaward-side water level and suspended sediment conditions and averaged wind speed and air temperature over the coastal transect. We extracted water level and wind conditions from high-frequency (10-minute or 15-minute) measurements for the three sites. Suspended sediment was extracted from high-frequency (15-minute) measurements for Hunter Estuary and from the global coastal Database for Impact and Vulnerability Analysis to sea-level rise (DIVA) (Schuerch et al., 2018; Vafeidis et al., 2008) for the other two sites. Daily air temperature was extracted from measurements for Venice Lagoon and Plum Island Estuary and the European Center for Medium-Range Weather Forecasts (ECMWF) Interim reanalysis (ERA-Interim) (Dee & Uppala, 2009) for Hunter Estuary. For each site, we constructed its 1-D transect from high-resolution Digital Elevation Model (DEM) and land cover maps (Hopkinson & Valentine, 2005; Rodríguez et al., 2017; Tambroni & Seminara, 2012; Ye & Pontius, 2016) by: 1) dividing all grid cells into 17 elevation groups spanning from -12.5 m to 16.5 m (some elevation groups can be empty); 2) calculating the average slope and land cover fractions of each elevation group; 3) calculating the transect length of each elevation group based on its slope and elevation range. For the first step, the elevation range of the 17 groups is the largest (i.e., 4 m) near to the land and sea edges and the smallest (i.e., 0.5 m) near to the sea level. For the third step, the slope of a grid cell is calculated by dividing its elevation by its distance to the nearest river network. The constructed 1-D transects of the three sites are shown in Figure 4.

Table 2. Characteristics and observational data of the three coastal wetland sites.

Site Name	Location	Tidal range	Wetland	Evaluation data	Data source
Venice Lagoon	45°33′N/12°27′E	0.84 m	Salt marshes	Water level, significant wave height, suspended sediment, bottom shear stress, long-term mineral accretion, long-term OM accretion	Bellucci et al. (2007); Carniello et al. (2011, 2012); Roner et al. (2016)
Plum Island Estuary	42°49′N/70°49′W	4.45 m	Salt marshes	Water level, suspended sediment, aboveground biomass, long-term mineral accretion, long-term OM accretion	Coleman & Kirwan (2020); Giblin (2018, 2019); Morris & Sundberg (2006, 2020); Vallino (2018); Wang et al. (2019); Wilson et al. (2014)
Hunter Estuary	32°55′S/151°48′E	1.11 m	Mangroves, salt marshes	Water level, suspended sediment, long-term mineral accretion, long-term OM accretion	Howe et al. (2009); Sandi et al. (2018); Rodríguez et al. (2017)

For Venice Lagoon, we used observed water level, suspended sediment and significant wave height and benchmark bottom shear stress estimates from a 2-D hydrodynamic model Wind Wave Tidal Model (WWTM) (Carniello et al., 2011) at two tidal flat stations (1BF: -1.1 masl; 2BF: -2.1 masl) for model evaluation. For Plum Island Estuary, we used observed water level at the channel (-0.73 masl) and marsh edge (1.25 masl) of Nelson Island, observed suspended sediment at the channel (-1.45 masl) and marsh interior (1.69 masl) of Law's Point, observed mineral accretion at three saltmarsh stations (LAC: a *Spartina alterniflora*-dominated high saltmarsh with an elevation of 1.1 masl; LPC: a *Spartina patens*-dominated high saltmarsh with an elevation of 1.4 masl; MRS: a *Spartina alterniflora*-dominated high saltmarsh with an elevation of 0.89 masl), and observed aboveground biomass at LAC and MRS for model evaluation. For Hunter Estuary, we used benchmark estimates of water level and suspended sediment at four stations (channel: 0.22 mAHD; mangrove edge: 0.05 mAHD; mangrove interior: 0.38 mAHD; saltmarsh edge: 0.65 mAHD) of the wetland for model evaluation. For a specific site, when validating our model over a station, we always chose the grid cell with the closest elevation to the station for comparison. For the model, mineral accretion is defined as the long-term average of net sediment deposition in the units of kg m^{-2} yr^{-1} and OM accretion is defined as the long-term average of net OM deposition in the units of kg C m^{-2} yr^{-1}. To compare with the observed mineral accretion, the modeled long-term average of net sediment deposition is divided by sediment bulk density.

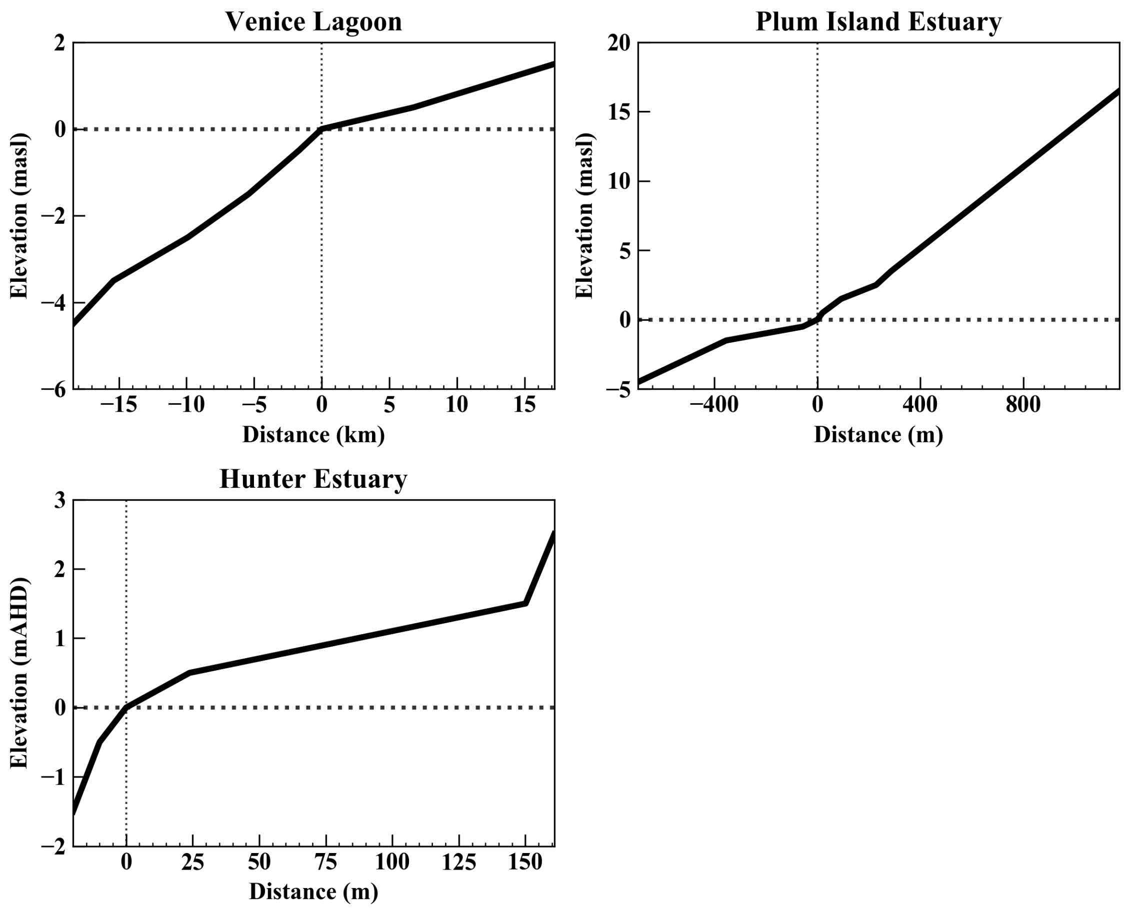

Figure 4. The elevation of 1-D MACES transects (solid lines) for Venice Lagoon, Plum Island Estuary and Hunter Estuary. Horizontal dash lines represent sea levels and vertical dash lines represent the ocean edge of coastal wetland.

3. Results

3.1. Venice Lagoon

Modeled hydrodynamics at Venice Lagoon were validated during two periods (12/10/2002–12/11/2002 and 4/2/2003–4/4/2003) when the boundary conditions were very different (Figure 5). The high tide and maximum wind speed in the second period were 64 cm asl and 17.3 m s^{-1}, respectively, which are much larger than those (38 cm asl

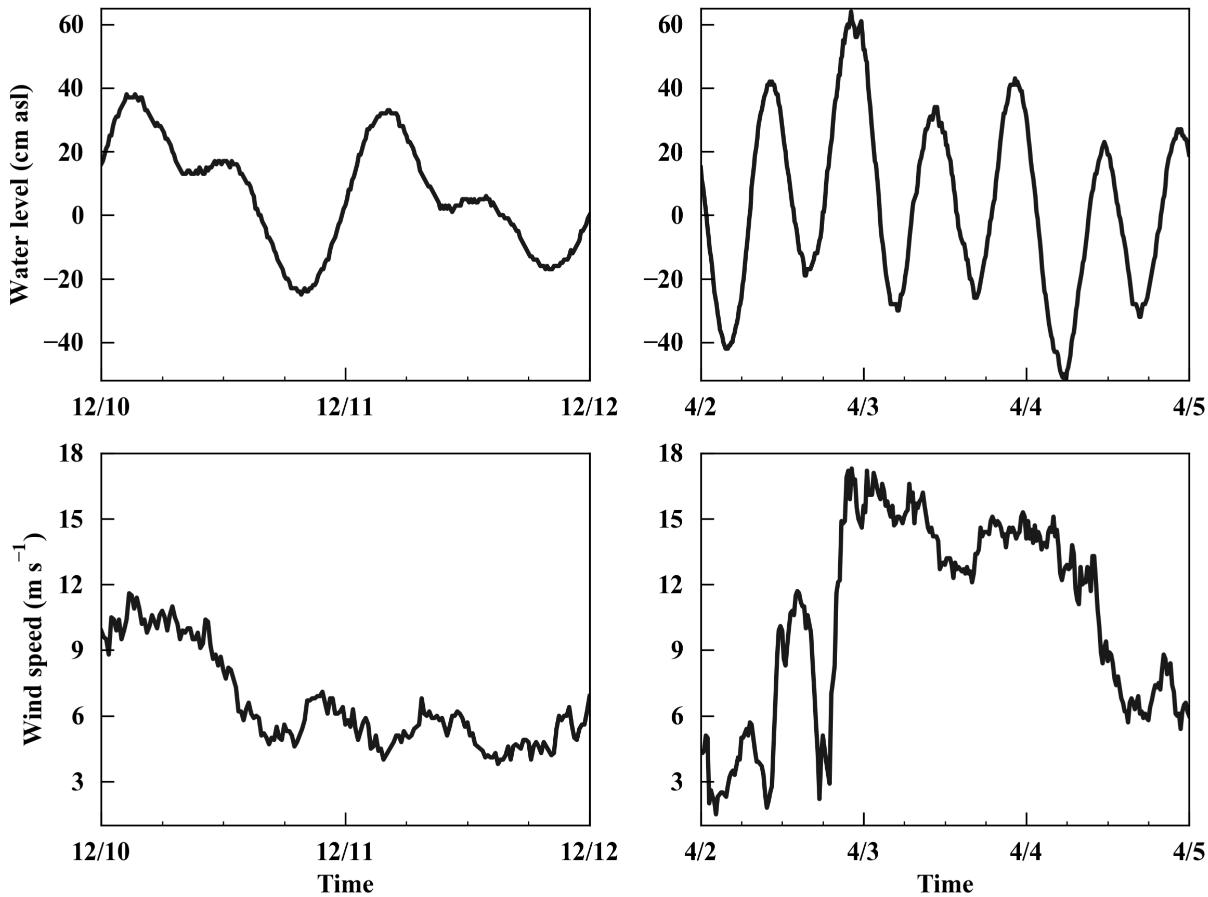

Figure 5. Measured water level and wind speed at the seaward boundary of Venice Lagoon during two time periods: 12/10/2002–12/11/2002 and 4/2/2003–4/4/2003.

and 11.6 m s^{-1}) of the first period. As shown in Figure 6, MACES-hydro performs well in reproducing the observed tide and wave dynamics in both periods. The root-mean-square-errors (RMSE) of simulated water depth at 1BF and 2BF during the low wind and tide period are 5.8 cm and 4.2 cm, respectively, which correspond to only 5% and 2% of the observed mean water depth. The RMSE of simulated significant wave height at 1BF and 2BF during the low wind and tide period are 4.7 cm and 4.6 cm, respectively, which correspond to 35% and 19% of the observed mean significant wave height. During the morning of 12/10/2002, when wind speed exceeded 11 m s^{-1}, the simulated significant wave height reached its peak value at the two stations: 22.6 cm and 39.4 cm, respectively. Correspondingly, the simulated bottom shear stress also reached its peak value at the two stations: 0.19 Pa and 0.31 Pa, respectively. During the high wind and tide period, the simulated significant wave height and bottom shear stress are much higher, which probably drove substantial sediment resuspension over tidal flats. On April 3, 2003, when wind speed frequently exceeded 15 m s^{-1}, the simulated significant wave height reached

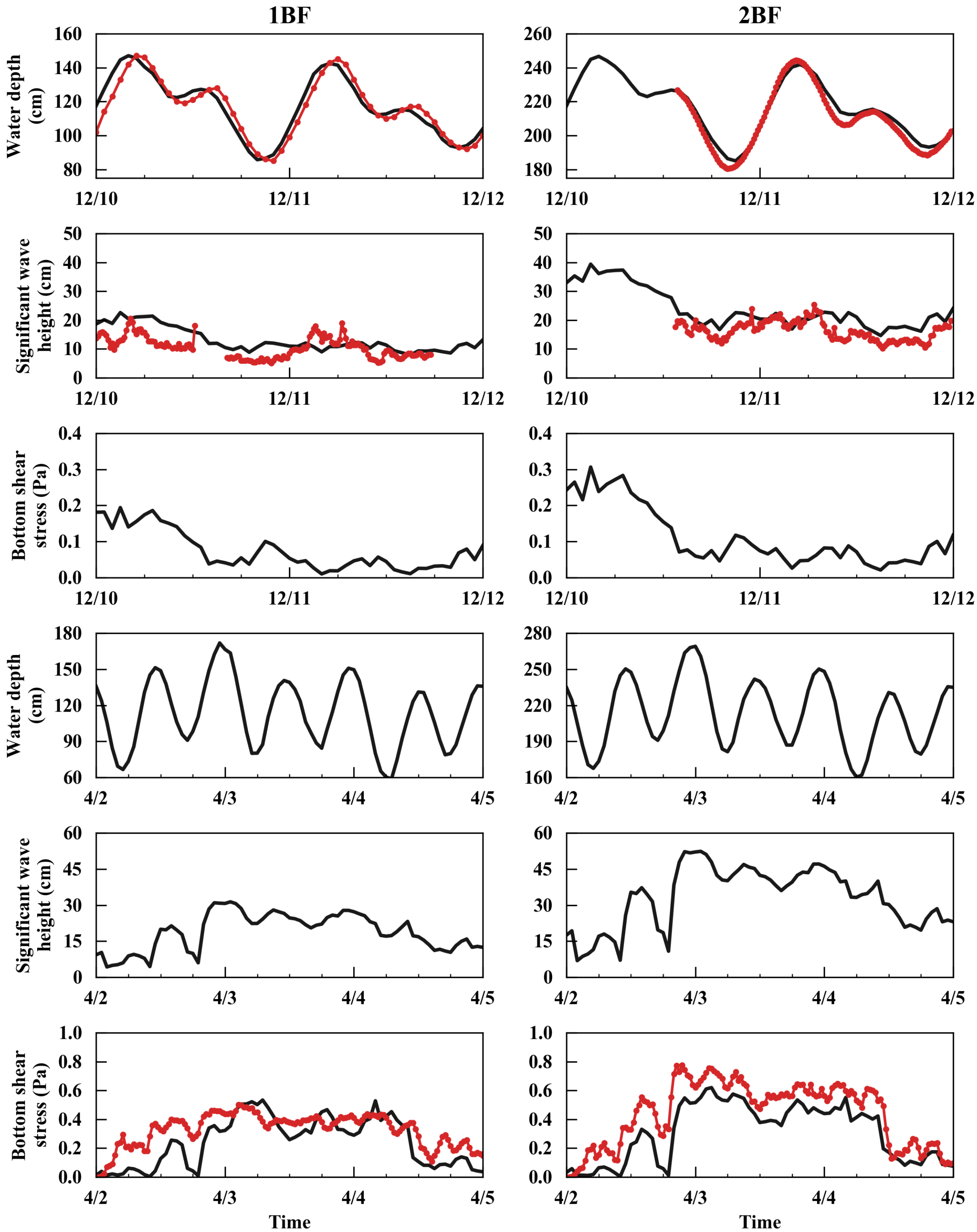

Figure 6. Dynamics of simulated (black) and observed or benchmark (red) water level, significant wave height and bottom shear stress at the two stations (1BF and 2BF) of Venice Lagoon during two time periods: 12/10/2002–12/11/2002 and 4/2/2003–4/4/2003.

its peak value at the two stations: 31.4 cm and 52.4 cm, respectively. The difference of significant wave height between 1BF and 2BF should be mainly attributed to the attenuation of wave energy by friction during the wave movement toward land. As shown in Figure 6, the model well reproduced the temporal variability of the benchmark estimated bottom shear stress at 1BF and 2BF during the high tide and wind period, with RMSE of 0.13 Pa and 0.15 Pa, respectively. In particular, by comparing the temporal variability of simulated bottom shear stress, significant wave height and water depth, we found that the wave component dominated the generation of the bottom shear stress in the high wind and tide period. Notably, the benchmark estimates are based on the simulation of WWTM instead of observations, so evaluation of the simulated bottom shear stress is marked by some uncertainty.

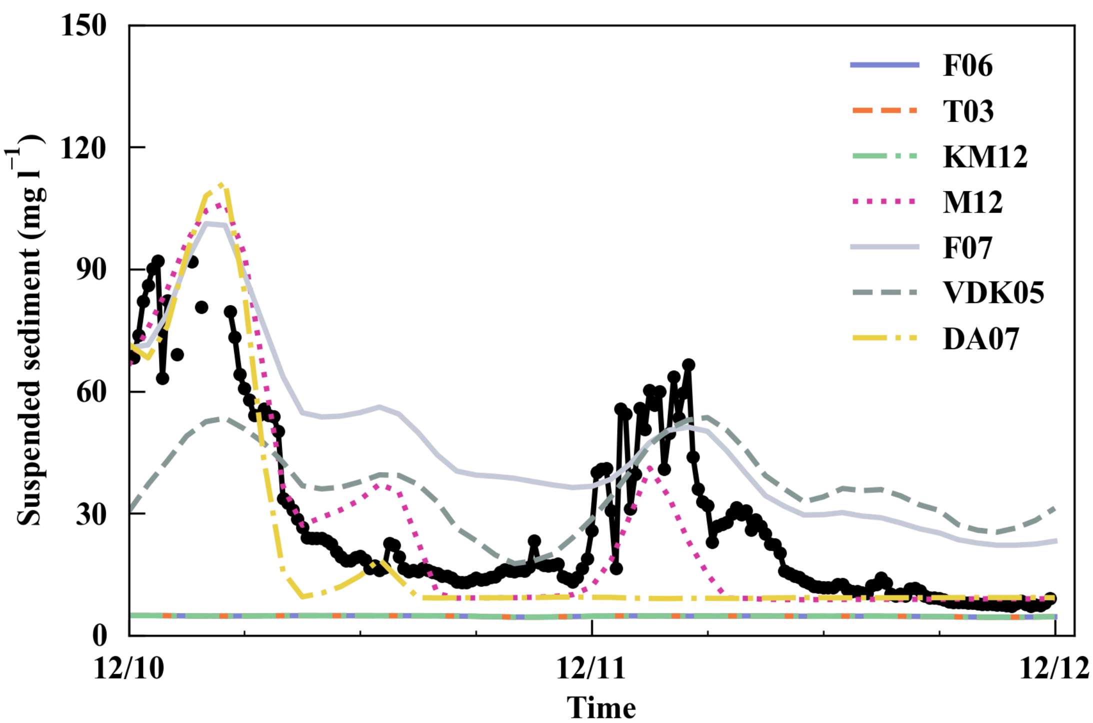

Figure 7. Comparison of observed column-integrated suspended sediment concentration (black) with simulated suspended sediment concentration simulated by seven mineral accretion algorithms at the 1BF station of Venice Lagoon during 12/10/2002–12/11/2002.

During the low wind and tide period, the observed suspended sediment concentration at 1BF ranged from 7.3 mg l^{-1} to 92.0 mg l^{-1} (Figure 7), with one larger peak value occurring in the turbulent morning of 12/10/2002 (Figure 5) and one smaller peak value occurring in the morning of 12/11/2002. As shown in the figure, the dynamics of simulated suspended sediment varied remarkably among the seven MACES-geomor mineral accretion algorithms (OM accretion algorithm is fixed at DA07). Only three algorithms (M12, F07 and VDK05) reproduced the observed two peak values of suspended sediment. Among them, the algorithm M12 has the lowest RMSE of 12.5 mg l^{-1}. Notably, previous studies also demonstrated that the dynamics of suspended sediment in the coast is notoriously difficult to model (Le Hir et al., 2007; Temmerman et al., 2003). The algorithm DA07 only simulated the larger peak suspended sediment concentration in the observations. The simulated suspended sediment by F06, T03 and KM12 is almost constant because these algorithms do not represent the sediment resuspension process. In MACES, we set the suspended sediment concentration in F06, T03 and KM12 at the site's reference value (9.4 mg l^{-1}) which was extracted from the DIVA database.

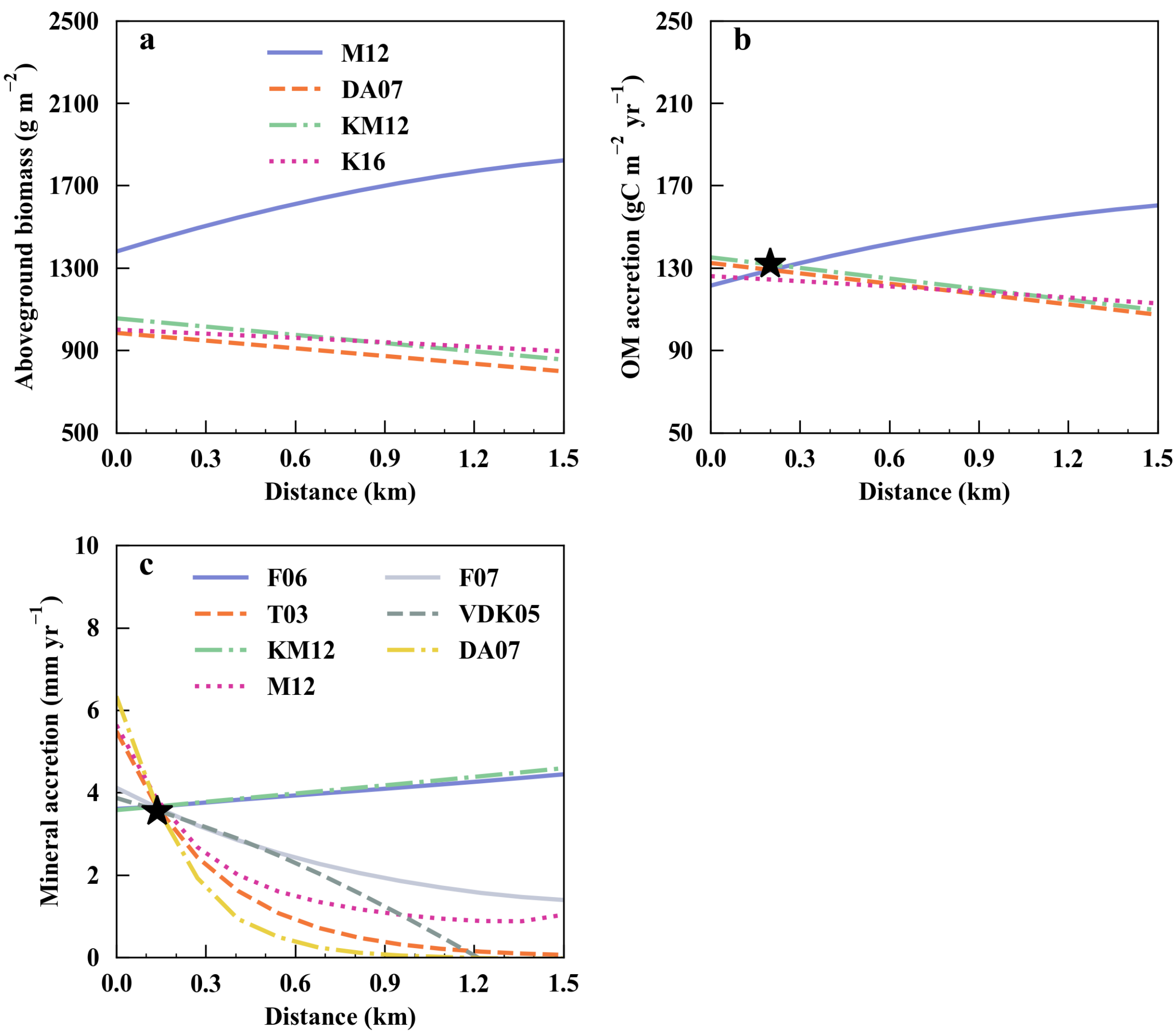

Figure 8. Comparison of the MACES-geomor algorithms in simulating mean plant aboveground biomass in July 2002 (a), mean annual OM accretion during 2002–2003

(b), and mean annual mineral accretion during 2002–2003 (c) over the saltmarsh of Venice Lagoon. Black stars in the subplots represent observations.

With calibration, all MACES-geomor algorithms can predict the observed long-term mineral (3.54 mm yr^{-1}) and OM accretion rate (132 gC m^{-2} yr^{-1}) at the observation station of Venice Lagoon (Figure 8). Also, the maximum aboveground biomass of saltmarsh species at Venice Lagoon simulated by the OM accretion algorithms M12, DA07, KM12 and K16 were 1821 gC m^{-2} yr^{-1}, 1000 gC m^{-2} yr^{-1}, 1055 gC m^{-2} yr^{-1} and 1016 gC m^{-2} yr^{-1}, respectively, which are within the range of 1–3 kg m^{-2} reported by Tambroni & Seminara (2012). Although the simulated mineral accretion by different algorithms converge at the observation station, their elevation and gradient across the transect of the saltmarsh platform differ importantly (Figure 8c). For the algorithm F06 and KM12, the simulated mineral accretion increased moderately along the elevation gradient from the saltmarsh edge to the inland area. This is because the suspended sediment concentration was kept at a constant value in the two algorithms while the bottom shear stress declined with water depth along the elevation gradient. For T03, because sediment deposition is modeled to decrease exponentially with the increase of elevation and distance, the simulated mineral accretion decreased along the elevation gradient from the saltmarsh edge to the inland area. For the other algorithms (M12, F07, VDK05 and DA07), their simulated mineral accretion also decreased along the elevation gradient, because strong sediment deposition and weak sediment resuspension over the vegetated saltmarsh caused a decline of suspended sediment concentration when tidal water advanced landward. Notably, although the simulated mineral accretion by the five algorithms (T03, M12, F07, VDK05 and DA07) all displays a negative relationship with distance, it differs remarkably among the algorithms at different locations. For example, at the saltmarsh edge, the simulated mineral accretion rate by DA07 was over 6 mm yr^{-1} but the value by VDK05 was less than 4 mm yr^{-1}. Similarly, the simulated OM accretion by the four OM accretion algorithms also varied differently over the saltmarsh platform (Figure 8b). In M12, OM accretion was larger in the more landward portions of the saltmarsh, but in the other three algorithms, it was larger at the saltmarsh edge. As shown in Figure 8a, this spatial difference could be mainly driven by the distinct spatial variability of simulated saltmarsh aboveground biomass of these algorithms.

3.2. Plum Island Estuary

The simulated hydrodynamics at Plum Island Estuary were validated in both summer and fall periods (7/19/2017–7/22/2017 and 10/7/2017–10/10/2017) when the boundary conditions were different (Figure 9). In the summer period, the tide level varied substantially, while the wind speed never exceeded 6 m s^{-1}. In contrast, in the fall period, the wind speed sometimes exceeded 8 m s^{-1}, while the tide level varied moderately. For both periods, MACES-hydro predicted the dynamics of water depth at both a river channel station (-0.73 masl) and a saltmarsh station (1.25 masl) accurately (Figure 10). The RMSE of the simulated water depth at the river channel station were 9.1 cm for the summer period and 7.5 cm for the fall period. The RMSE of the simulated water depth at the saltmarsh station were 2.2 cm for the summer period and 1.5 cm for the fall period.

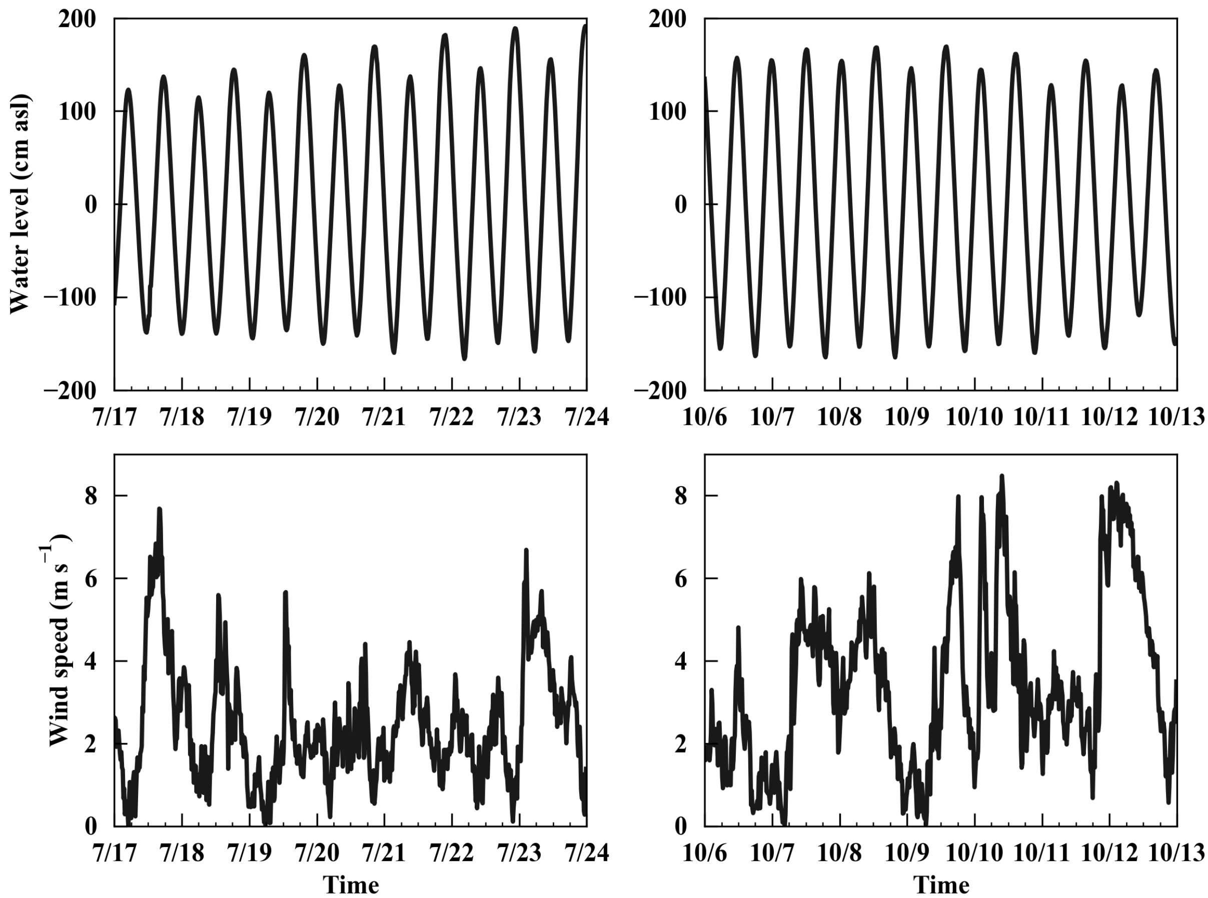

Figure 9. Measured water level and wind speed at the seaward boundary of Plum Island Estuary during two time periods: 7/17/2017–7/23/2017 and 10/6/2017–10/12/2017.

Suspended sediment simulated by MACES-hydro was validated at a river channel station (-1.45 masl) and a saltmarsh station (1.69 masl) of Plum Island Estuary for the summer period (Figure 11). The model did not reproduce the dynamics of suspended sediment at the two stations well, which further emphasizes the challenge of modeling suspended sediment over the coastal wetland landscape (Le Hir et al., 2007; Temmerman et al., 2003). Among the algorithms, the simulated suspended sediment by F06, T03 and KM12 was set at the site's reference value (2.7 mg l^{-1}) extracted from the DIVA database. The simulated suspended sediment by F07 and VDK05 has similar magnitude compared to the observations but the temporal variability of the simulation and observations differed. As mentioned in previous studies (Le Hir et al., 2007; Temmerman et al., 2003), the spatial heterogeneity of sediment and vegetation characteristics could be the major causes for the low simulation accuracy presented here. Additionally, two limitations in the model could also be responsible for the poor simulation skill: 1) the 1-D MACES-hydro model does not represent channel processes and the 1-D discretization also probably does not reproduce accurately the site domain; and 2) we lack data to set the sediment flux across the seaward boundary for this site.

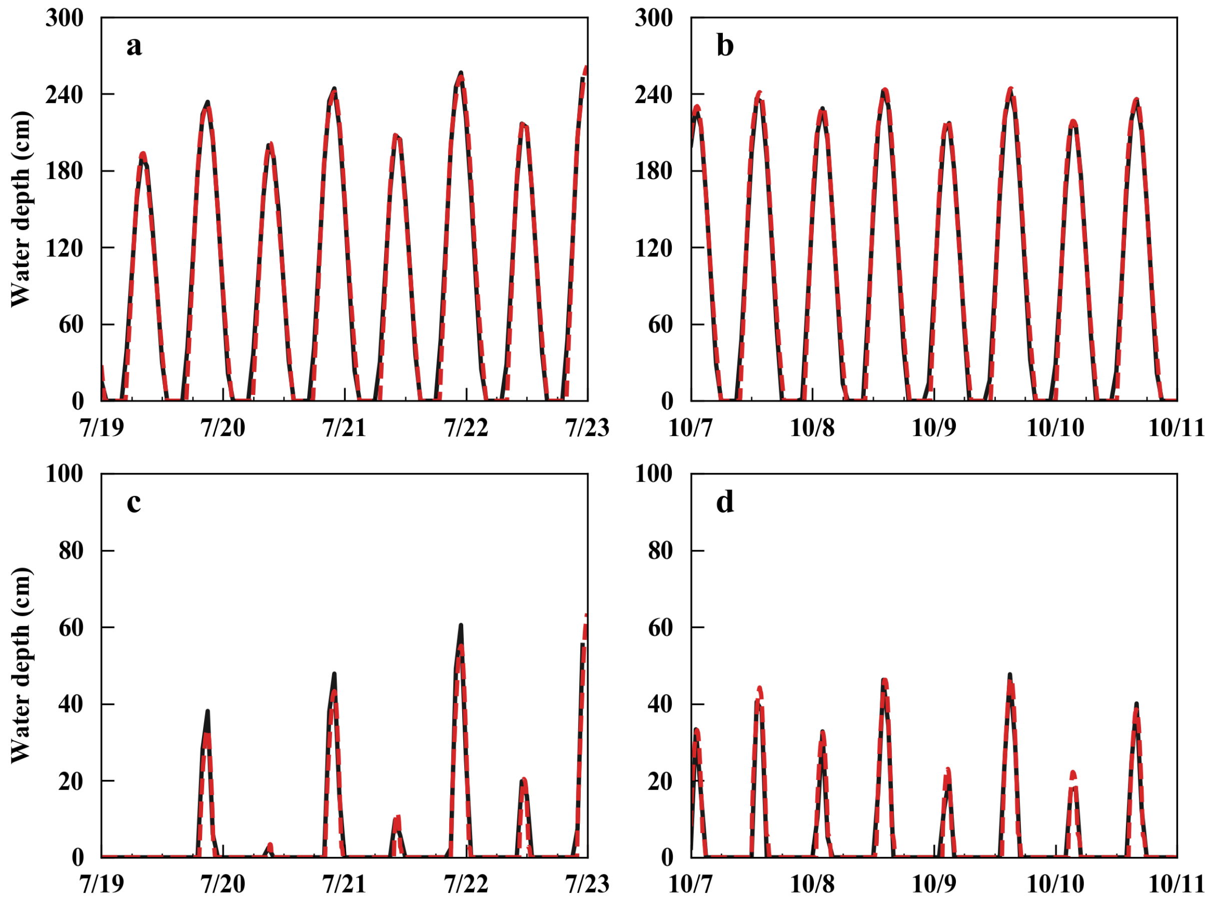

Figure 10. Comparison of simulated (black) and observed (red) water depth at the channel station at an elevation of -1.45 masl (a and b) and the *Spartina*-dominated saltmarsh station at an elevation of 1.69 masl (c and d) in Plum Island Estuary during two time periods: 7/19/2017–7/22/2017 and 10/7/2017–10/10/2017.

Despite the limitations in modeling suspended sediment, the MACES-geomor algorithms can still well reproduce the observed mineral accretion, aboveground biomass and OM accretion at stations of different elevations and saltmarsh species (Figures 12–13). As shown in Figure 11a, the mineral accretion algorithms T03, M12 and VDK05 accurately predicted the decrease of mineral accretion from the tall *Spartina alterniflora*-dominated low saltmarsh at an elevation of 0.89 masl (MRS: 6.9±0.9 mm yr^{-1}) to the *Spartina alterniflora*-dominated high saltmarsh at an elevation of 1.1 masl (LAC: 5.3±0.1 mm yr^{-1})

to the *Spartina patens*-dominated high saltmarsh at an elevation of 1.4 masl (LPC:

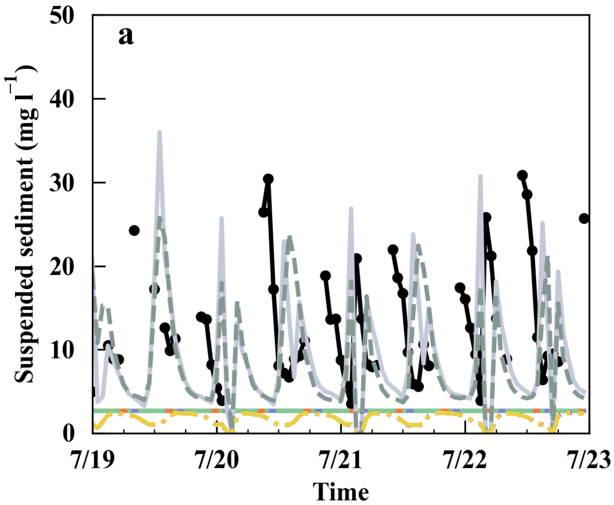

Figure 11. Comparison of observed column-integrated suspended sediment concentration (black) with suspended sediment concentration simulated by seven mineral accretion algorithms at the channel station at an elevation of -1.45 masl (a) and the *Spartina*-dominated saltmarsh station at an elevation of 1.69 masl (b) in Plum Island Estuary during the period of 7/19/2017–7/22/2017.

2.3±0.1 mm yr^{-1}). The algorithm F07 predicted the mineral accretion at the MRS and LAC stations but underestimated the mineral accretion at the LPC station. The algorithm DA07 overestimated the mineral accretion at the MRS station but correctly predicted it at the LAC and LPC stations. As discussed in Section 3.1, because the concentration of suspended sediment was set at a constant value in F06 and KM12 and the bottom shear stress declined with the advance of tide water, the simulated mineral accretion by these two algorithms was slightly larger in the saltmarsh interior. All the OM accretion algorithms successfully predicted the elevation gradient of the mean aboveground biomass of saltmarsh species in July 2018 (Figure 12b). They also successfully predicted the observed mean OM accretion (69.9±9.4 gC m^{-2} yr^{-1}) of the saltmarsh within the elevation range of 0–1.5 masl (Figure 13). We also tested how the model simulated the seasonality of aboveground biomass at the LAC station, which is a *Spartina alterniflora*-dominated high saltmarsh (Figure 12c). Among the four OM accretion algorithms, only DA07 and KM12 represent the seasonal variability of aboveground biomass using sinusoidal functions of month or day of year. As shown in the figure, this sinusoidal-function-based approach performed much better in simulating the aboveground biomass of saltmarsh in summer and fall but severely overestimated it in spring.

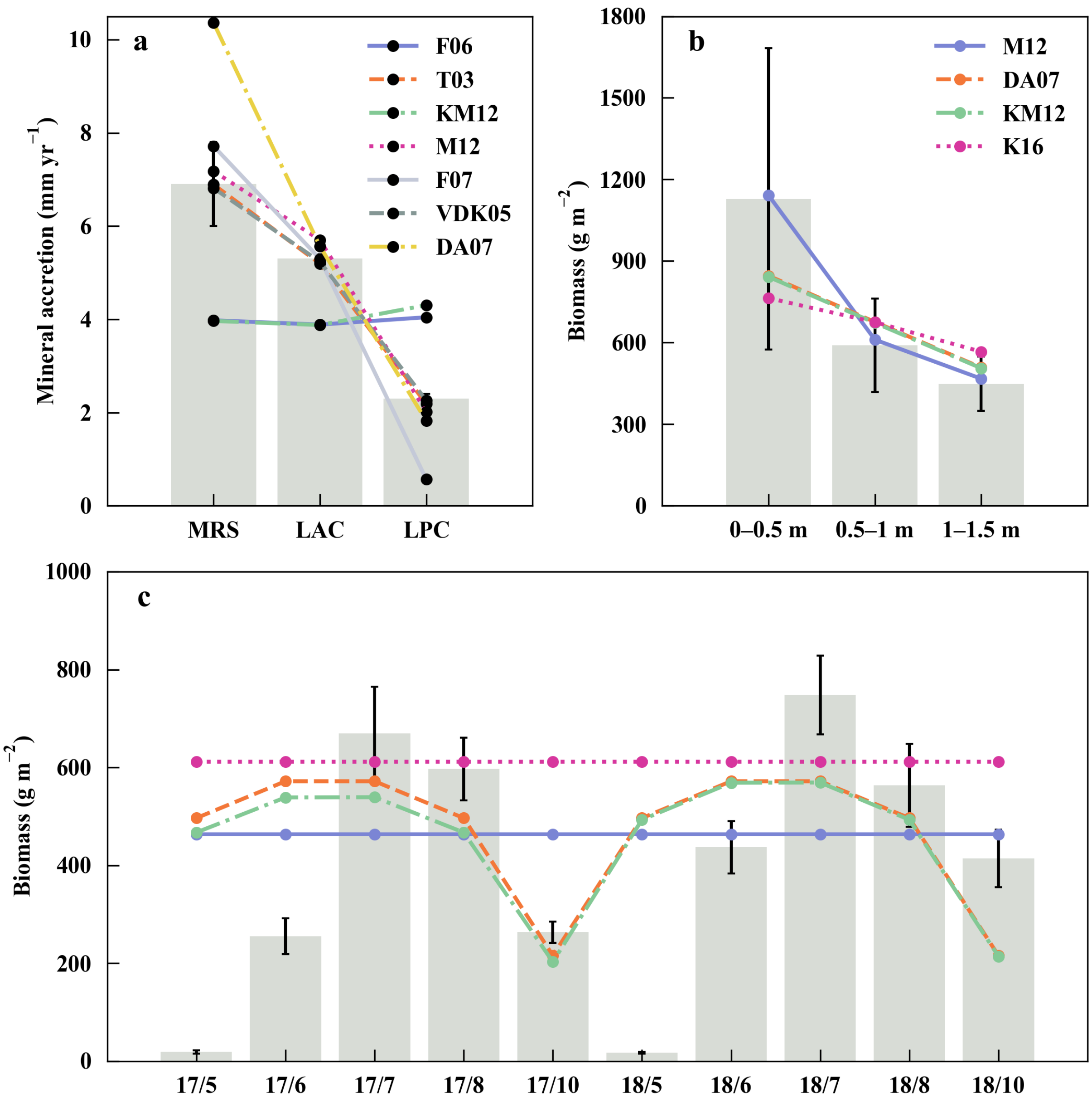

Figure 12. Comparison of the MACES-geomor algorithms in simulating mean annual mineral accretion at the station MRS, LAC and LPC during 2017–2018 (a), mean plant aboveground biomass in July 2018 at three elevation ranges (b), and monthly mean plant aboveground biomass during 2017–2018 at the LAC station (c). Bars in the subplots represent observations.

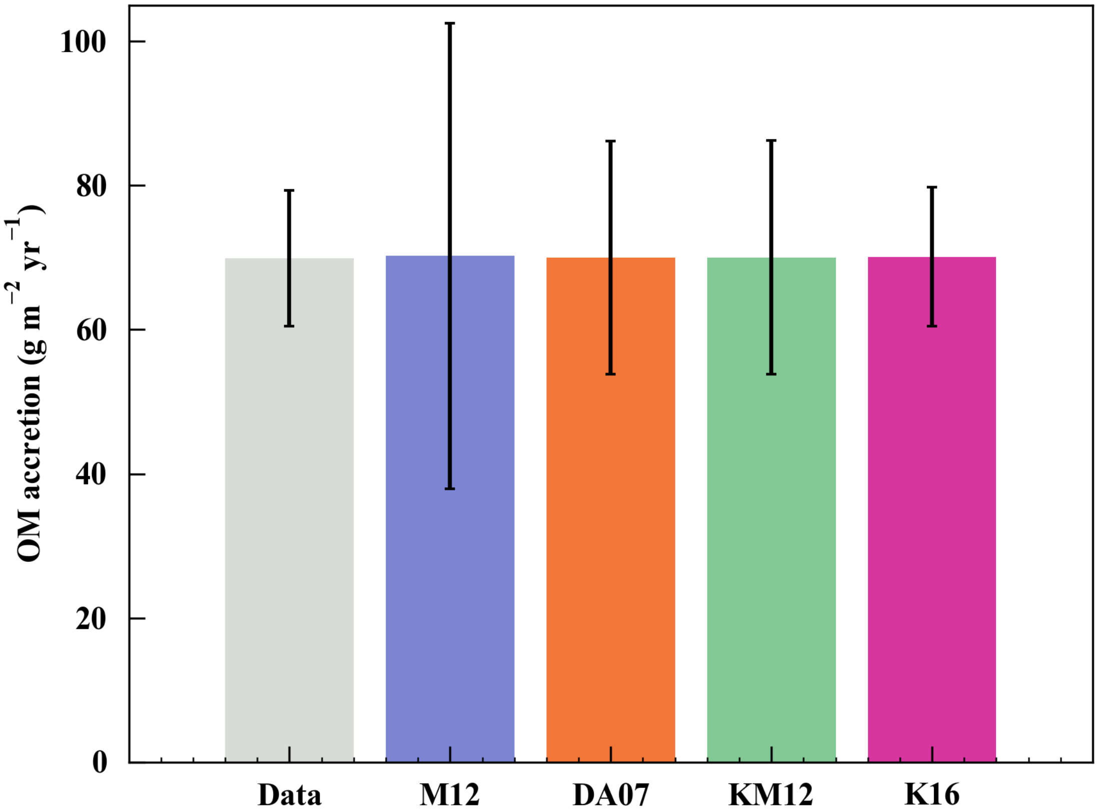

Figure 13. Comparison of simulated and observed average OM accretion within the elevation range of 0–1.5 m at the saltmarsh of Plum Island during 2017–2018. M12, DA07, KM12 and K16 are four different OM algorithms.

3.3. Hunter Estuary

The hydrodynamics simulated at Hunter Estuary where the tidal range mangrove species reside in low elevations and saltmarsh species reside in high elevations were validated in the period of 9/28/2004–9/30/2004 with dynamic water level and suspended sediment boundary conditions (Figures 14a and 14b). During the period, MACES-hydro well reproduced the benchmark estimated water depth at four representative locations of the wetland: a river channel station at an elevation of -0.22 mAHD (Figure 14c), a mangrove-dominated station at an elevation of 0.05 mAHD (Figure 14d), a mangrove-dominated interior station at an elevation of 0.38 mAHD (Figure 14e), and a saltmarsh-dominated station at an elevation of 0.65 mAHD (Figure 14f). The RMSE of the simulated water depth at the four stations are 4.6 cm, 5.4 cm, 2.7 cm and 0.4 cm, respectively.

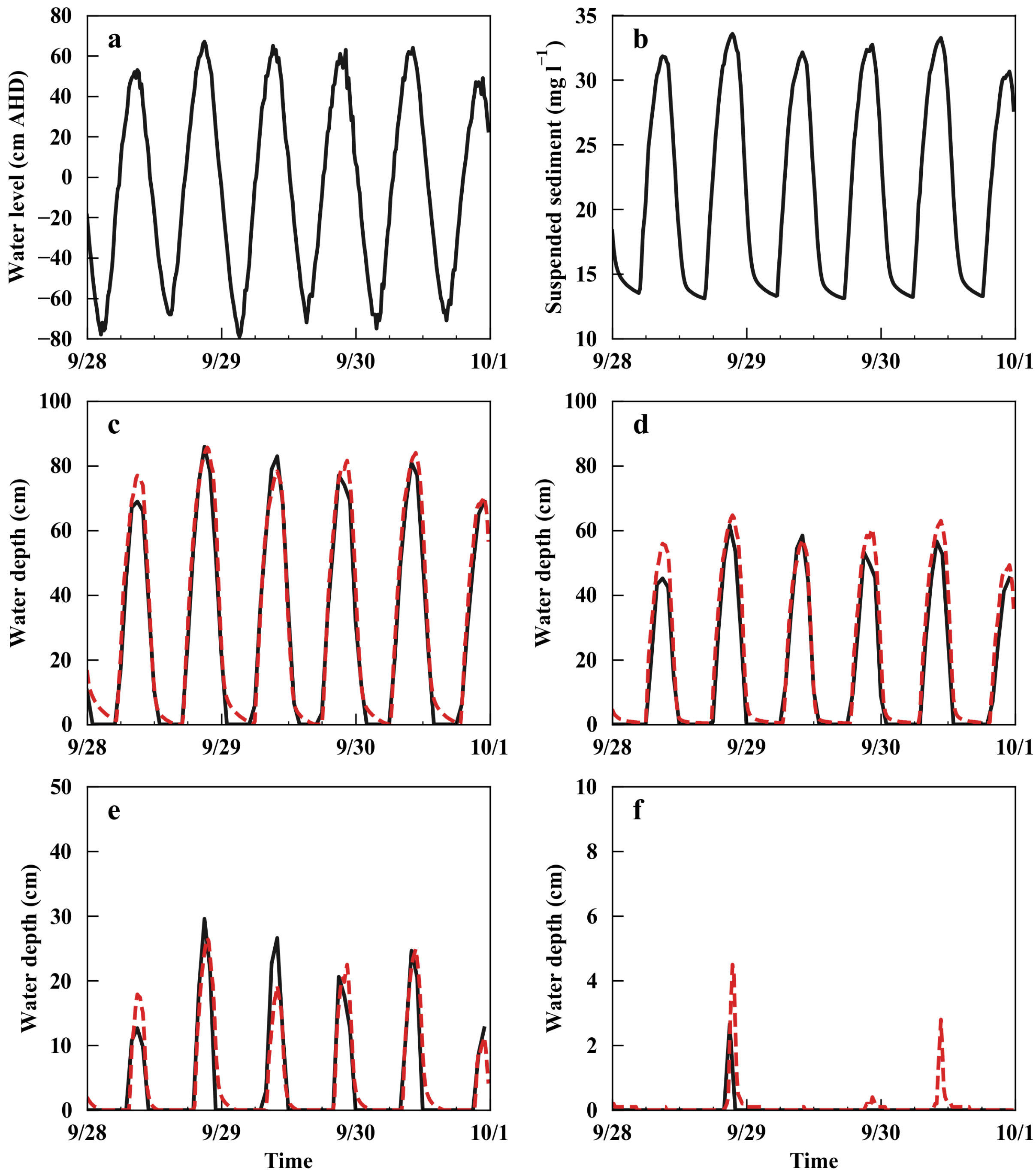

Figure 14. Measured water level (a) and suspended sediment concentration (b) at the seaward boundary of Hunter Island Estuary and comparison of simulated (black) and benchmark (red) water depth at the channel station at an elevation of -0.22 mAHD (c), the mangrove edge station at an elevation of 0.05 mAHD (d), the mangrove interior station at an elevation of 0.38 mAHD (e) and the saltmarsh edge station at an elevation of 0.65 mAHD (f) in Hunter Estuary during 9/28/2004–9/30/2004.

By accounting for the sediment flux from the river inlet of the wetland site (Figure 14b), MACES-geomor performed much better in simulating the dynamics of suspended sediment at the Hunter Estuary wetland than that at the Plum Island Estuary wetland (Figure 15). In particular, the RMSE of the simulated suspended sediment by the algorithm F07 at the four stations mentioned above from low to high elevation are only 1.8 mg l^{-1}, 2.0 mg l^{-1}, 2.5 mg l^{-1} and 0.3 mg l^{-1}, respectively (we removed data points in the comparison when the simulated water depth was zero). The algorithms M12 and DA07 also simulated the reduction of suspended sediment with the advance of tide water due to sediment deposition. However, it is clear that in these two algorithms, the trapping capability of wetland vegetation on suspended sediment is probably underestimated. For the algorithms F06, T03 and KM12, as their simulated suspended sediment is not influenced by sediment deposition, the dynamics of suspended sediment were fully controlled by the boundary conditions. For the algorithm VDK05, although its simulated suspended sediment is influenced by sediment deposition, the deposition rate seemed to be strongly underestimated at the Hunter Estuary wetland.

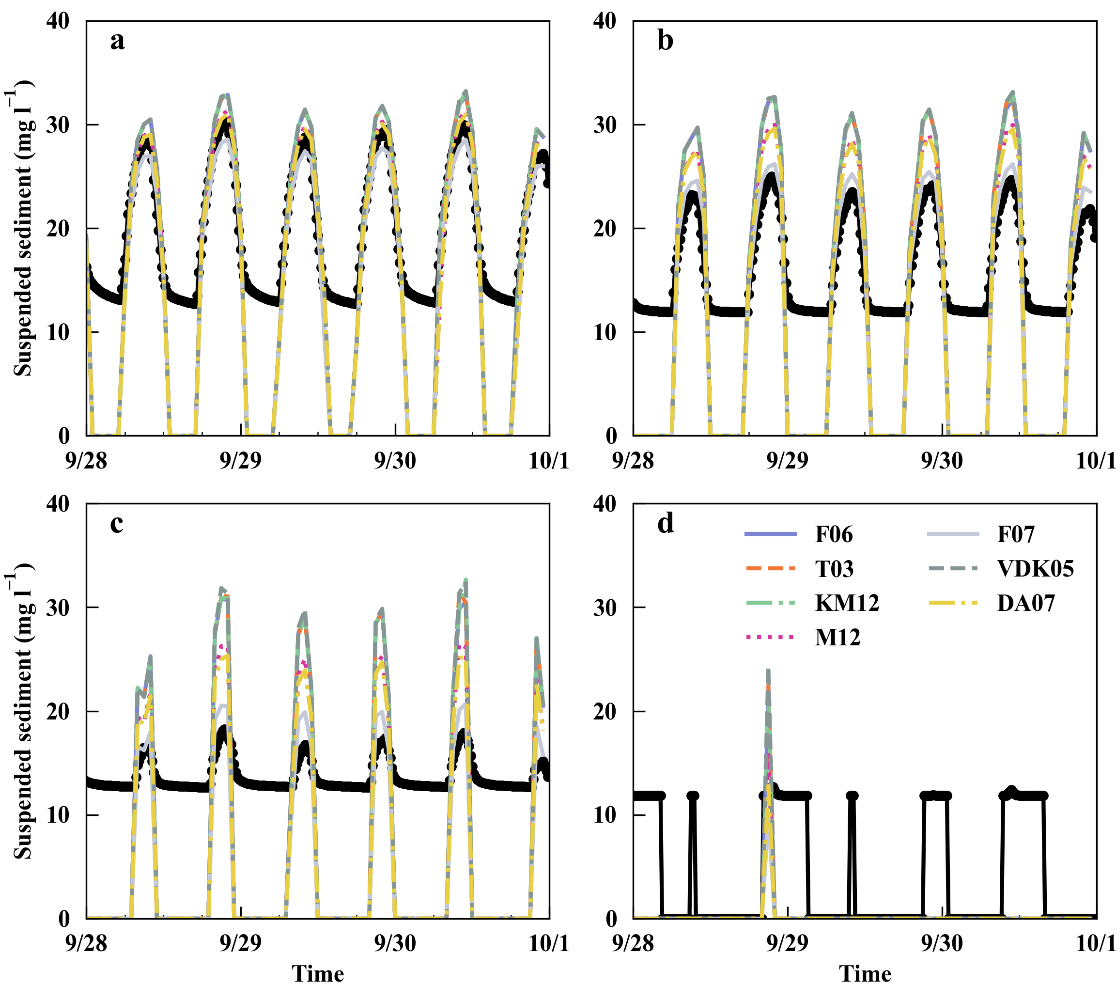

Figure 15. Comparison of observed column-integrated suspended sediment concentration (black) with suspended sediment concentration simulated by seven mineral accretion algorithms at the channel station at an elevation of -0.22 mAHD (a), the mangrove edge station at an elevation of 0.05 mAHD (b), the mangrove interior station at an elevation of 0.38 mAHD (c) and the saltmarsh edge station at an elevation of 0.65 mAHD (d) in Hunter Estuary during 9/28/2004–9/30/2004.

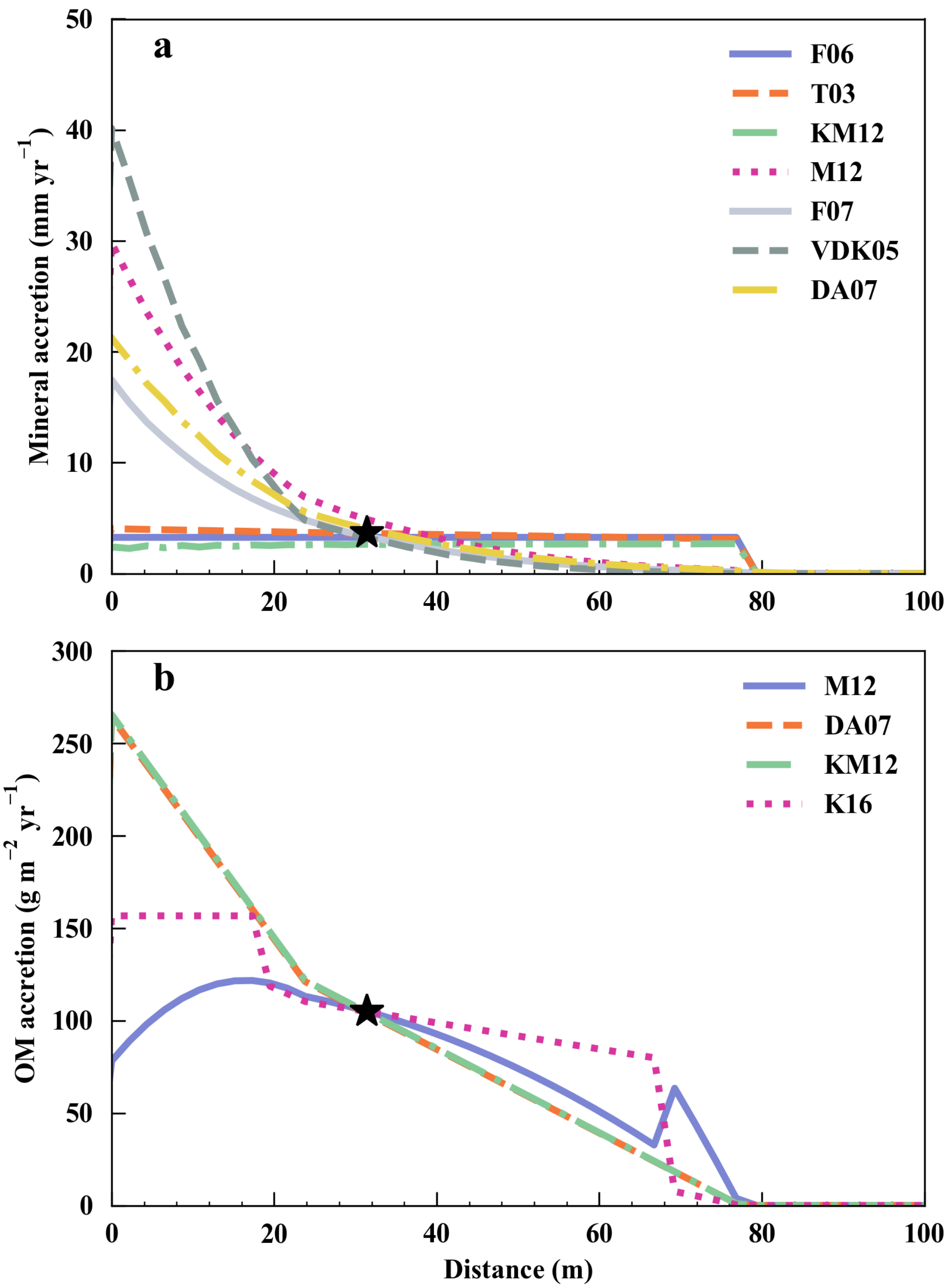

Figure 16. Comparison of the MACES-geomor algorithms in simulating mean annual mineral accretion (a) and mean annual OM accretion (b) at the mangrove-dominated station at an elevation of 0.56 mAHD in Hunter Estuary in 2004. Black stars in the subplots represent observations.

With calibration, the MACES-geomor algorithms successfully predicted the observed long-term mineral accretion (3.66 mm yr^{-1}) and OM accretion (105 gC m^{-2} yr^{-1}) at a mangrove-dominated station at an elevation of 0.56 mAHD in Hunter Estuary (Figure 16). As discussed in Section 3.1, although the simulated mineral accretion from all the mineral accretion algorithms converges at the observation location, their elevation and distance gradient across the wetland platform differ importantly (Figure 16a). For the algorithms F06, T03 and KM12, the simulated mineral accretion only changed moderately within the tidal range of the wetland. For the other algorithms, the simulated mineral accretion declined strongly with the increase of elevation and distance, showing the reduction of suspended sediment from the wetland edge to the interior area due to deposition. As such, the simulated mineral accretion at the wetland edge differs remarkably among these algorithms. Similarly, the elevation and distance gradient of simulated OM accretion are very different among the OM accretion algorithms (Figure 16b). In MACES-geomor, the spatial variability of simulated OM accretion is mainly controlled by two factors: plant aboveground biomass and root:shoot quotient. For example, for M12, because the aboveground biomass is modeled as a quadratic function and the root:shoot quotient of saltmarsh species is higher than that of mangrove species (Kakeh et al., 2016), the simulated OM accretion reached a maximum value at the wetland interior and increased at the mangrove-saltmarsh boundary.

4. Discussion

4.1. Application of MACES to coastal wetlands of diverse environments

Coastal wetlands are an important ecosystem type spanning broad geographic regions, from tropical and subtropical mangroves, midlatitude saltmarshes to arctic coastal tundra (Keddy, 2000). Through the comprehensive validations described above, we showed that the multiple-algorithm model framework we developed has the potential to predict the eco-geomorphology of coastal wetlands in diverse environments. First, the three validation sites are representative for a large spectrum of coastal wetlands on earth. They include the most common plant species of coastal wetlands that were widely studied for assessing the response of ecosystem to SLR (Crase et al., 2013; Day Jr et al., 1999; Kirwan & Mudd, 2012; Liu et al., 2020; Morris et al., 2002; Mudd et al., 2010; Temmerman et al., 2003b): *Spartina alterniflora*, *Spartina patens*, *Puccinellia palustris*, *Spartina maritima* and *Avicennia marina*. These three sites are also located in zones of different tidal ranges (microtidal and macrotidal) and climate (Mediterranean climate, humid continental climate and humid subtropical climate). Additionally, very few modeling studies of eco-geomorphology have included both saltmarshes and mangroves. Second, our model accurately predicted the dynamics of water depth over the entire wetland domain for all the three sites. Accurate simulation of water depth over the wetland domain is important for projection of many wetland eco-geomorphological processes such as mineral accretion, primary production and landward migration under future SLR (Kirwan & Mudd, 2012; Reyes et al., 2000; Rodríguez et al., 2017). Third, beyond the prediction of mineral and OM accretion at single locations, the model framework is also able to predict the elevation and distance gradient of mineral and OM accretion over the wetland domain.

Importantly, a particular advantage of this multiple-algorithm framework is that it allows the selection of appropriate eco-geomorphology algorithms for coastal wetlands of different environments. As the model validations implied, it is very unlikely that single algorithms of mineral accretion, OM accretion and other eco-geomorphological processes can work well for all coastal wetlands across the globe. Instead, a possibly better strategy is to use data to inform the selection of different optimal algorithms for coastal wetlands of different environments. Currently, there have already been many published datasets of mineral and OM accretion from coastal wetlands across broad regions (Breithaupt et al., 2012; Chmura et al., 2003; Crosby et al., 2016; Lovelock et al., 2015; Parkinson et al., 2017). The next step would be to identify and survey geographic and ecological factors that are crucial for the classification of coastal wetlands. We believe that the development of this multiple-algorithm coastal wetland eco-geomorphology framework can greatly facilitate this optimization strategy in global applications.

4.2. Impacts of algorithm-level uncertainties on modeling coastal wetland eco-geomorphology

Our numerical experiments at the three coastal wetland sites revealed substantial algorithm-level uncertainties in mineral and OM accretion models that could have significant impacts on the projection of the response of coastal wetlands to future environmental changes. For example, since landscape elevation usually increases from the wetland edge to the interior area, more sediment may be trapped at the edge of coastal wetlands to buffer the influence of SLR. As indicated in the analysis of Plum Island Estuary, mineral accretion algorithms that simulate clear elevation gradients of sediment deposition probably provide more realistic projections of mineral accretion and thus the ecosystem's habitat change. In contrast, although F06 and KM12 were widely used in previous studies (French, 2006; Kirwan & Mudd, 2012; Schuerch et al., 2013; Temmerman et al., 2003a), they would likely underestimate the capability of saltmarshes to cope with SLR if sediment supply is sufficient because they simulate nearly uniform sediment deposition within the vegetated periodically flooded area. Also, comparing the elevation gradient of the simulated mineral and OM accretion, many algorithms simulated an increase of the ratio of OM accretion to mineral accretion with elevated topography, implying a larger impact of OM accretion to the geomorphological dynamics of coastal wetlands in the interior areas. But this spatial pattern does not exist for the mineral accretion algorithms F06 and KM12.

Besides SLR, macroclimatic drivers (particularly air temperature) are also important for coastal wetland vulnerability assessments to climate change (Osland et al., 2016). In the OM accretion algorithms, only DA07 and KM12 represent the seasonality of coastal wetland vegetation growth. Further, only KM12 represents the response of vegetation growth to air temperature. For algorithms that do not represent the seasonality of vegetation growth, they would inevitably overestimate sediment deposition, OM deposition and the shoreline protection potential of coastal wetlands in the cold seasons (Schoutens et al., 2019). Importantly, they are unable to fully resolve the impact of climate warming on the vulnerability of coastal wetlands.

Based on our model validations, there are two possible approaches to reduce the algorithm-level uncertainty in the simulation of coastal wetland evolution. First, it is important to constrain mineral and OM accretion models using observations from at least two locations with different elevations and vegetation species in a wetland site. New observations should be prioritized to capture such gradients. Second, as discussed in the above section, it is better to choose optimal algorithms based on the unique environment of specific coastal wetlands. We believe that these approaches would help resolve contradicting predictions on coastal wetland evolution under accelerated SLR (Craft et al., 2009; Kirwan et al., 2010, 2016; Rodríguez et al., 2017; Schuerch et al., 2018).

4.3. Limitations and future development

The model validations reported here showed that the dynamics of suspended sediment cannot always be well reproduced by MACES. As discussed in Section 3.2, this model deficiency could be caused by the ignoring of channel processes in the 1-D hydrodynamic framework and also the possibly imperfect delineation of the coastal wetland transects. Since the dynamics of suspended sediment is controlled by some factors that are extremely heterogeneous, rather than improving the process parameterizations directly, a better strategy may be to use satellite-based suspended sediment data to drive mineral accretion algorithms, such as the satellite-borne GlobColour data (http://globcolour.info). To improve the delineation of the coastal wetland transect, we plan to use the high-quality coastal Digital Elevation Model (CoastalDEM) (Kulp & Strauss, 2018) and the high-resolution global distribution map of mangroves and saltmarshes compiled by US Geological Survey and the World Conservation and Monitoring Centre (http://data.unep-wcmc.org/) for global applications.

Another limitation in the model is the poor representation of aboveground biomass in cold seasons. Based on our analysis, this is mainly due to the use of simple sinusoidal functions to represent the response of vegetation growth to temperature. To assess how this model uncertainty affects the simulation of coastal wetland evolution, we will include more comprehensive representations of coastal wetland phenology as those implemented in more complex land surface models (Oleson et al., 2013).

5. Acknowledgements

This research is part of the PREMIS Initiative at Pacific Northwest National Laboratory (PNNL). It was conducted under the Laboratory Directed Research and Development Program at PNNL, a multi-program national laboratory operated by Battelle for the U.S. Department of Energy under Contract DE-AC05-76RL01830. The authors wish to thank the Ministero delle Infrastrutture e dei Trasporti, Magistrato alle Acque di Venezia, through its concessionary Consorzio Venezia Nuova for the field data collected in the Venice lagoon. Data sets of Plum Island Estuary were provided by the Plum Island Ecosystems LTER, with the support by the National Science Foundation under Grants #OCE-9726921, OCE-0423565, OCE-1058747, OCE-1238212, OCE-1637630. The data used in this study will be publicly available through the PNNL DataHub repository (https://data.pnnl.gov/). The MACES source code can be freely downloaded from https://doi.org/10.5281/zenodo.4029425.

6. References

Aburto-Oropeza, O., Ezcurra, E., Danemann, G., Valdez, V., Murray, J., & Sala, E. (2008). Mangroves in the Gulf of California increase fishery yields. *Proceedings of the National Academy of Sciences*, **105**, 10456–10459.

Bellucci, L. G., Frignani, M., Cochran, J. K., Albertazzi, S., Zaggia, L., Cecconi, G., & Hopkins, H. (2007). ^{210}Pb and ^{137}Cs as chronometers for salt marsh accretion in the Venice Lagoon–links to flooding frequency and climate change. *Journal of Environmental Radioactivity*, **97**, 85–102.

Blum, M. D., & Roberts, H. H. (2009). Drowning of the Mississippi Delta due to insufficient sediment supply and global sea-level rise. *Nature Geoscience*, **2**, 488–491.

Breithaupt, J. L., Smoak, J. M., Smith, T. J., Sanders, C. J., & Hoare, A. (2012). Organic carbon burial rates in mangrove sediments: Strengthening the global budget. *Global Biogeochemical Cycles*, **26**, GB3011.

Burden, R. L., Faires, J. D., & Reynolds, A. C. (1978). *Numerical Analysis* (pp. 254). Boston: Prindle, Weber and Schmidt Inc.

Carniello, L., Defina, A., Fagherazzi, S., & D'Alpaos, L. (2005). A combined wind wave–tidal model for the Venice lagoon, Italy. *Journal of Geophysical Research: Earth Surface*, **110**, F04007.

Carniello, L., D'Alpaos, A., & Defina, A. (2011). Modeling wind waves and tidal flows in shallow micro-tidal basins. *Estuarine, Coastal and Shelf Science*, **92**, 263–276.

Carniello, L., Defina, A., & D'Alpaos, L. (2012). Modeling sand-mud transport induced by tidal currents and wind waves in shallow microtidal basins: Application to the Venice Lagoon (Italy). *Estuarine, Coastal and Shelf Science*, **102**, 105–115.

Chmura, G. L., Anisfeld, S. C., Cahoon, D. R., & Lynch, J. C. (2003). Global carbon sequestration in tidal, saline wetland soils. *Global Biogeochemical Cycles*, **17**, 1111.

Coleman, D., & Kirwan, M. (2020). PIE LTER suspended sediments at Law's Point, West Creek, a tidal marsh and creek off the Rowley River, Rowley, MA, during 2016-2017. Environmental Data Initiative.

Craft, C., Clough, J., Ehman, J., Joye, S., Park, R., Pennings, S., ... & Machmuller, M. (2009). Forecasting the effects of accelerated sea-level rise on tidal marsh ecosystem services. *Frontiers in Ecology and the Environment*, **7**, 73–78.

Crase, B., Liedloff, A., Vesk, P. A., Burgman, M. A., & Wintle, B. A. (2013). Hydroperiod is the main driver of the spatial pattern of dominance in mangrove communities. *Global Ecology and Biogeography*, **22**, 806–817.

Crosby, S. C., Sax, D. F., Palmer, M. E., Booth, H. S., Deegan, L. A., Bertness, M. D., & Leslie, H. M. (2016). Salt marsh persistence is threatened by predicted sea-level rise. *Estuarine, Coastal and Shelf Science*, **181**, 93–99.

D'Alpaos, A., Lanzoni, S., Marani, M., & Rinaldo, A. (2007). Landscape evolution in tidal embayments: Modeling the interplay of erosion, sedimentation, and vegetation dynamics. *Journal of Geophysical Research: Earth Surface*, **112**, F01008.

D'Alpaos, A., Carniello, L., & Mudd, S. M. (2011). Dynamic response of marshes to perturbations in suspended sediment concentrations and rates of relative sea level rise. *Journal of Geophysical Research: Earth Surface*, **116**, F04020.

Day Jr, J. W., Rybczyk, J., Scarton, F., Rismondo, A., Are, D., & Cecconi, G. (1999). Soil accretionary dynamics, sea-level rise and the survival of wetlands in Venice Lagoon: a field and modelling approach. *Estuarine, Coastal and Shelf Science*, **49**, 607–628.

Dee, D. P., & Uppala, S. (2009). Variational bias correction of satellite radiance data in the ERA-Interim reanalysis. *Quarterly Journal of the Royal Meteorological Society*, **135**, 1830–1841.

Deegan, L. A., Johnson, D. S., Warren, R. S., Peterson, B. J., Fleeger, J. W., Fagherazzi, S., & Wollheim, W. M. (2012). Coastal eutrophication as a driver of salt marsh loss. *Nature*, **490**, 388–392.

Doherty, J., Brebber, L., & Whyte, P. (1994). *PEST: Model-independent parameter estimation* (Vol. 122). Corinda, Australia: Watermark Computing.

Donatelli, M., Bregaglio, S., Confalonieri, R., De Mascellis, R., & Acutis, M. (2014). A generic framework for evaluating hybrid models by reuse and composition–A case study on soil temperature simulation. *Environmental Modelling & Software*, **62**, 478–486.

Fagherazzi, S., Palermo, C., Rulli, M. C., Carniello, L., & Defina, A. (2007). Wind waves in shallow microtidal basins and the dynamic equilibrium of tidal flats. *Journal of Geophysical Research: Earth Surface*, **112**, F02024.

Fagherazzi, S., Kirwan, M. L., Mudd, S. M., Guntenspergen, G. R., Temmerman, S., D'Alpaos, A., ... & Clough, J. (2012). Numerical models of salt marsh evolution: Ecological, geomorphic, and climatic factors. *Reviews of Geophysics*, **50**, RG1002.

Fisher, R. A., & Koven, C. D. (2020). Perspectives on the future of land surface models and the challenges of representing complex terrestrial systems. *Journal of Advances in Modeling Earth Systems*, **12**, e2018MS001453.

French, J. (2006). Tidal marsh sedimentation and resilience to environmental change: exploratory modelling of tidal, sea-level and sediment supply forcing in predominantly allochthonous systems. *Marine Geology*, **235**, 119–136.

Giblin, A. (2018). Year 2017, PIE LTER wind sensor data, 15 minute intervals, from the Ipswich Bay Yacht Club pier located in Ipswich, MA Environmental Data Initiative.

Giblin, A. (2019). PIE LTER marsh water table height, logging data from the Nelson Island Spartina marsh site, Rowley, MA for May-October 2017. Environmental Data Initiative.

Guseva, S., Bleninger, T., Jöhnk, K., Polli, B. A., Tan, Z., Thiery, W., ... & Stepanenko, V. (2020). Multimodel simulation of vertical gas transfer in a temperate lake. *Hydrology and Earth System Sciences*, **24**, 697–715.

Hopkinson, C., & Valentine, V. (2005). PIE LTER 2005 Digital elevation model for the Plum Island Sound estuary, Massachusetts, filtered_grd, last filtered grid - Raster Environmental Data Initiative.

Howe, A. J., Rodríguez, J. F., & Saco, P. M. (2009). Surface evolution and carbon sequestration in disturbed and undisturbed wetland soils of the Hunter estuary, southeast Australia. *Estuarine, Coastal and Shelf Science*, **84**, 75–83.

Howes, N. C., FitzGerald, D. M., Hughes, Z. J., Georgiou, I. Y., Kulp, M. A., Miner, M. D., ... & Barras, J. A. (2010). Hurricane-induced failure of low salinity wetlands. *Proceedings of the National Academy of Sciences*, **107**, 14014–14019.

Huntzinger, D. N., Schwalm, C., Michalak, A. M., Schaefer, K., King, A. W., Wei, Y., ... & Berthier, G. (2013). The North American Carbon Program Multi-Scale Synthesis and Terrestrial Model Intercomparison Project – Part 1: Overview and experimental design. *Geoscientific Model Development*, **6**, 2121–2133.

Jin, Z., Zhuang, Q., Tan, Z., Dukes, J. S., Zheng, B., & Melillo, J. M. (2016). Do maize models capture the impacts of heat and drought stresses on yield? Using algorithm ensembles to identify successful approaches. *Global Change Biology*, **22**, 3112–3126.

Kakeh, N., Coco, G., & Marani, M. (2016). On the morphodynamic stability of intertidal environments and the role of vegetation. *Advances in Water Resources*, **93**, 303–314.

Keddy, P. A. (2000). *Wetland ecology: principles and conservation*. Cambridge, UK: Cambridge University Press.

Kirwan, M. L., Guntenspergen, G. R., d'Alpaos, A., Morris, J. T., Mudd, S. M., & Temmerman, S. (2010). Limits on the adaptability of coastal marshes to rising sea level. *Geophysical Research Letters*, **37**, L23401.

Kirwan, M. L., & Mudd, S. M. (2012). Response of salt-marsh carbon accumulation to climate change. *Nature*, **489**, 550–553.

Kirwan, M. L., & Megonigal, J. P. (2013). Tidal wetland stability in the face of human impacts and sea-level rise. *Nature*, **504**, 53–60.

Kirwan, M. L., Temmerman, S., Skeehan, E. E., Guntenspergen, G. R., & Fagherazzi, S. (2016). Overestimation of marsh vulnerability to sea level rise. *Nature Climate Change*, **6**, 253–260.

Kulp, S. A., & Strauss, B. H. (2018). CoastalDEM: A global coastal digital elevation model improved from SRTM using a neural network. *Remote Sensing of Environment*, **206**, 231–239.

Kurganov, A., & Levy, D. (2002). Central-upwind schemes for the Saint-Venant system. *ESAIM: Mathematical Modelling and Numerical Analysis*, **36**, 397–425.

Le Hir, P., Monbet, Y., & Orvain, F. (2007). Sediment erodability in sediment transport modelling: Can we account for biota effects?. *Continental Shelf Research*, **27**, 1116-1142.

Leonardi, N., Ganju, N. K., & Fagherazzi, S. (2016). A linear relationship between wave power and erosion determines salt-marsh resilience to violent storms and hurricanes. *Proceedings of the National Academy of Sciences*, **113**, 64–68.

Liang, Q., & Marche, F. (2009). Numerical resolution of well-balanced shallow water equations with complex source terms. *Advances in water resources*, **32**, 873–884.

Liao, C., Zhuang, Q., Leung, L. R., & Guo, L. (2019). Quantifying dissolved organic carbon dynamics using a three-dimensional terrestrial ecosystem model at high spatial-temporal resolutions. *Journal of Advances in Modeling Earth Systems*, **11**, 4489– 4512.

Liu, W., Chen, X., Strong, D. R., Pennings, S. C., Kirwan, M. L., Chen, X., & Zhang, Y. (2020). Climate and geographic adaptation drive latitudinal clines in biomass of a widespread saltmarsh plant in its native and introduced ranges. *Limnology and Oceanography*, **65**, 1399–1409.

Lovelock, C. E., Cahoon, D. R., Friess, D. A., Guntenspergen, G. R., Krauss, K. W., Reef, R., ... & Saintilan, N. (2015). The vulnerability of Indo-Pacific mangrove forests to sea-level rise. *Nature*, **526**, 559–563.

Maan, D. C., Van Prooijen, B. C., Wang, Z. B., & De Vriend, H. J. (2015). Do intertidal flats ever reach equilibrium?. *Journal of Geophysical Research: Earth Surface*, **120**, 2406–2436.

Maan, D. C., van Prooijen, B. C., & Wang, Z. B. (2019). Progradation speed of tide-dominated tidal flats decreases stronger than linearly with decreasing sediment availability and linearly with sea level rise. *Geophysical Research Letters*, **46**, 262–271.

Marani, M., D'Alpaos, A., Lanzoni, S., Carniello, L., & Rinaldo, A. (2007). Biologically-controlled multiple equilibria of tidal landforms and the fate of the Venice lagoon. *Geophysical Research Letters*, **34**, L11402.

Macreadie, P. I., Anton, A., Raven, J. A., Beaumont, N., Connolly, R. M., Friess, D. A., ... & Lovelock, C. E. (2019). The future of Blue Carbon science. *Nature Communications*, **10**, 3998.

Mariotti, G., & Fagherazzi, S. (2010). A numerical model for the coupled long-term evolution of salt marshes and tidal flats. *Journal of Geophysical Research: Earth Surface*, **115**, F01004.

Mcleod, E., Poulter, B., Hinkel, J., Reyes, E., & Salm, R. (2010). Sea-level rise impact models and environmental conservation: A review of models and their applications. *Ocean & Coastal Management*, **53**, 507–517.

Morris, J. T., Sundareshwar, P. V., Nietch, C. T., Kjerfve, B., & Cahoon, D. R. (2002). Responses of coastal wetlands to rising sea level. *Ecology*, **83**, 2869–2877.

Morris, J., & Sundberg, K. (2006). Change in marsh surface elevation measured with a Surface Elevation Table (SET) at control plots in a *Spartina alterniflora*-dominated salt marsh at Law's Point, Rowley River, Plum Island Ecosystem LTER, MA. Environmental Data Initiative.

Morris, J. T., Edwards, J., Crooks, S., & Reyes, E. (2012). Assessment of carbon sequestration potential in coastal wetlands. In R. Lal, K. Lorenz, R. Huttl, B. U. Schneider, J. von Braun (Eds.), *Recarbonization of the biosphere: ecosystems and the global carbon cycle* (pp. 517–531). New York: Springer.

Morris, J., & Sundberg, K. (2020). Aboveground biomass data from control sites in a *Spartina alterniflora*-dominated salt marsh at Law's Point, Rowley River, Plum Island Ecosystem LTER, MA. Environmental Data Initiative.

Mudd, S. M., Fagherazzi, S., Morris, J. T., & Furbish, D. J. (2004). Flow, sedimentation, and biomass production on a vegetated salt marsh in South Carolina: Toward a predictive model of marsh morphologic and ecologic evolution. In S. Fagherazzi, M. Marani, & L. K. Blum (Eds.), *The ecogeomorphology of tidal marshes* (pp. 165–188). Washington, DC: American Geophysical Union (AGU).

Oleson, K. W., et al. (2013). *Technical description of version 4.5 of the Community Land Model (CLM); NCAR Tech*. Note NCAR/TN-503+STR; NCAR: Boulder, CO, 2013. DOI: 10.5065/D6RR1W7M

Osland, M. J., Enwright, N. M., Day, R. H., Gabler, C. A., Stagg, C. L., & Grace, J. B. (2016). Beyond just sea-level rise: Considering macroclimatic drivers within coastal wetland vulnerability assessments to climate change. *Global Change Biology*, **22**, 1–11.

Parkinson, R. W., Craft, C., DeLaune, R. D., Donoghue, J. F., Kearney, M., Meeder, J. F., ... & Turner, R. E. (2017). Marsh vulnerability to sea-level rise. *Nature Climate Change*, **7**, 756–756.

Reyes, E., White, M. L., Martin, J. F., Kemp, G. P., Day, J. W., & Aravamuthan, V. (2000). Landscape modeling of coastal habitat change in the Mississippi Delta. *Ecology*, **81**, 2331–2349.

Reyes, E., Martin, J. F., Day, J. W., Kemp, G. P., & Mashriqui, H. (2004). River forcing at work: Ecological modeling of prograding and regressive deltas. *Wetlands Ecology and Management*, **12**, 103–114.

Rodríguez, J. F., Saco, P. M., Sandi, S., Saintilan, N., & Riccardi, G. (2017). Potential increase in coastal wetland vulnerability to sea-level rise suggested by considering hydrodynamic attenuation effects. *Nature Communications*, **8**, 16094.

Roe, P. L. (1986). Characteristic-based schemes for the Euler equations. *Annual Review of Fluid Mechanics*, **18**, 337–365.

Roner, M., D'Alpaos, A., Ghinassi, M., Marani, M., Silvestri, S., Franceschinis, E., & Realdon, N. (2016). Spatial variation of salt-marsh organic and inorganic deposition and organic carbon accumulation: Inferences from the Venice lagoon, Italy. *Advances in Water Resources*, **93**, 276–287.

Sandi, S. G., Rodríguez, J. F., Saintilan, N., Riccardi, G., & Saco, P. M. (2018). Rising tides, rising gates: The complex ecogeomorphic response of coastal wetlands to sea-level rise and human interventions. *Advances in Water Resources*, **114**, 135–148.

Schellnhuber, H. J., Frieler, K., & Kabat, P. (2014). The elephant, the blind, and the intersectoral intercomparison of climate impacts. *Proceedings of the National Academy of Sciences*, **111**, 3225–3227.

Schoutens, K., Heuner, M., Minden, V., Schulte Ostermann, T., Silinski, A., Belliard, J. P., & Temmerman, S. (2019). How effective are tidal marshes as nature-based shoreline protection throughout seasons?. *Limnology and Oceanography*, **64**, 1750–1762.

Schuerch, M., Vafeidis, A., Slawig, T., & Temmerman, S. (2013). Modeling the influence of changing storm patterns on the ability of a salt marsh to keep pace with sea level rise. *Journal of Geophysical Research: Earth Surface*, **118**, 84–96.

Schuerch, M., Spencer, T., Temmerman, S., Kirwan, M. L., Wolff, C., Lincke, D., ... & Hinkel, J. (2018). Future response of global coastal wetlands to sea-level rise. *Nature*, **561**, 231–234.

Soulsby, R. L. (1997). *Dynamics of marine sands: A manual for practical applications* (248 pp.). London: Thomas Telford.

Tambroni, N., & Seminara, G. (2012). A one-dimensional eco-geomorphic model of marsh response to sea level rise: Wind effects, dynamics of the marsh border and equilibrium. *Journal of Geophysical Research: Earth Surface*, **117**, F03026.

Tan, Z., Zhuang, Q., & Walter Anthony, K. (2015). Modeling methane emissions from arctic lakes: Model development and site-level study. *Journal of Advances in Modeling Earth Systems*, **7**, 459–483.

Tan, Z., Leung, L. R., Li, H.-Y., & Tesfa, T. (2018). Modeling sediment yield in land surface and earth system models: Model comparison, development, and evaluation. *Journal of Advances in Modeling Earth Systems*, **10**, 2192–2213.

Temmerman, S., Govers, G., Meire, P., & Wartel, S. (2003a). Modelling long-term tidal marsh growth under changing tidal conditions and suspended sediment concentrations, Scheldt estuary, Belgium. *Marine Geology*, **193**, 151–169.

Temmerman, S., Govers, G., Wartel, S., & Meire, P. (2003b). Spatial and temporal factors controlling short-term sedimentation in a salt and freshwater tidal marsh, Scheldt estuary, Belgium, SW Netherlands. *Earth Surf. Processes Landforms*, **28**, 739–755.

Temmerman, S., Meire, P., Bouma, T. J., Herman, P. M., Ysebaert, T., & De Vriend, H. J. (2013). Ecosystem-based coastal defence in the face of global change. *Nature*, **504**, 79–83.

Teuchies, J., Vandenbruwaene, W., Carpentier, R., Bervoets, L., Temmerman, S., Wang, C., ... & Meire, P. (2013). Estuaries as filters: the role of tidal marshes in trace metal removal. *PLOS ONE*, **8**, e70381.

Vafeidis, A. T., Nicholls, R. J., McFadden, L., Tol, R. S., Hinkel, J., Spencer, T., ... & Klein, R. J. (2008). A new global coastal database for impact and vulnerability analysis to sea-level rise. *Journal of Coastal Research*, **24**, 917–924.

Vallino, J. (2018). PIE LTER, Hach, OTT RLS measurements of water column depth at 15 minute intervals in the lower Plum Island Sound off the Ipswich Bay Yacht Club pier, Ipswich, MA, year 2017 Environmental Data Initiative.

Van de Koppel, J., Van der Wal, D., Bakker, J. P., & Herman, P. M. J. (2005). Self-organization and vegetation collapse in salt marsh ecosystems. *The American Naturalist*, **165**, E1–E12.

Wang, F., Lu, X., Sanders, C. J., & Tang, J. (2019). Tidal wetland resilience to sea level rise increases their carbon sequestration capacity in United States. *Nature Communications*, **10**, 5434.

Ward, N. D., Megonigal, J. P., Bond-Lamberty, B., Bailey, V. L., Butman, D., Canuel, E. A., ... & Hopkinson, C. S. (2020). Representing the function and sensitivity of coastal interfaces in Earth system models. *Nature Communications*, **11**, 2458.

Wilson, C. A., Hughes, Z. J., FitzGerald, D. M., Hopkinson, C. S., Valentine, V., & Kolker, A. S. (2014). Saltmarsh pool and tidal creek morphodynamics: Dynamic equilibrium of northern latitude saltmarshes?. *Geomorphology*, **213**, 99–115.

Ye, S., & Pontius, R. G. (2016). PIE LTER Land Cover (2013), Plum Island Sound estuary, Massachusetts - Raster Environmental Data Initiative.

Pacific Northwest National Laboratory

902 Battelle Boulevard
P.O. Box 999
Richland, WA 99354
1-888-375-PNNL (7665)

www.pnnl.gov